The Thesis Committee for Antony Martin Harvey
Certifies that this is the approved version of the following thesis:

Evaluation of MRN Complex and ATM Protein-Protein Interactions using Cleavable DSSO Crosslinking and Mass Spectrometry

APPROVED BY
SUPERVISING COMMITTEE:

Supervisor:

Tanya T. Paull

Andreas T. Matouschek

Evaluation of MRN Complex and ATM Protein-Protein Interactions using Cleavable DSSO Crosslinking and Mass Spectrometry

by

Antony Martin Harvey

Thesis

Presented to the Faculty of the Graduate School of

The University of Texas at Austin

in Partial Fulfillment

of the Requirements

for the Degree of

Master of Arts

The University of Texas at Austin

December 2017

Dedication

This is dedicated to Kristi, whose unfaltering support enabled me to perform the proteomics research described in this thesis…

Acknowledgements

I would first like to thank my sponsors—my employer and managers—for affording me the time and resources to pursue studies in proteomics. I would like to thank my research supervisor, Tanya Paull, who provided me space in her lab, gave me advice and direction, and permitting me to explore new experimental approaches. I thank Dr. Andreas Matouschek for his unfailing enthusiasm and for taking the time to be the second reader of this thesis. I would also like to thank Dr. Edward Marcotte for taking the time to discuss protein crosslinking and for reading this thesis, and the staff in the Proteomics Facility: Dr. Maria Person, Michelle Gadush and Andre Bui, who helped me optimize the MS instrument method and acquired the mass spectrometry data from the crosslinking experiments.

I would be remiss if I did not also acknowledge the current and former members of the Paull Lab who helped me around the lab and taught me the cell biology techniques I used in my research: Gary Kao, Ji-Hoon Lee, Michael Mand, Logan Myler, Nicolette Ender, Nodar Makharashvili, Rajashree Deshpande, Rose Stewart, Seung Woo Ryu, Tanya Raymond, Yi Zhou, and Yizhi Yin.

Lastly, I must thank my friends and family who never ceased in encouraging me to further my education!

Abstract

Evaluation of MRN Complex and ATM Protein-Protein Interactions using Cleavable DSSO Crosslinking and Mass Spectrometry

Antony Martin Harvey, MA

The University of Texas at Austin, 2017

Supervisor: Tanya T. Paull

Ataxia telangiectasia (A–T) is an inherited autosomal recessive disorder caused by mutations in the ataxia telangiectasia mutated (ATM) gene. The canonical role of ATM is to induce cell checkpoint arrest following DNA damage. When cells experience DNA double-strand breaks (DSBs), the Mre11-Rad50-Nbs1 (MRN) complex senses the damage, activating ATM, which mobilizes a protective signaling cascade, activating the cell cycle checkpoint, arresting cell growth. If the extent of damage is excessive, the apoptotic pathway is activated; otherwise DNA repair is initiated using either homologous recombination (HR) or through non-homologous end joining (NHEJ).

ATM also plays a key role in redox homeostasis. Loss of this cellular function results in the misfolding and aggregation of proteins. Misfolded proteins are degraded by three pathways: the ubiquitin proteasome system (UPS), macroautophagy and chaperone-mediated autophagy (CMA). Aggregated proteins that are resistant to these protein clearance mechanisms can form inclusion bodies, which can lead to neurodegeneration.

The primary approach used for investigating protein interactions in this research was with the DSSO cleavable crosslinking technique: first to evaluate the MRN protein complex structure and protein-protein interactions; then to elucidate ATM binding partners in cells undergoing oxidative stress.

The results of the MRN complex *in vitro* crosslinking experiment were that 53 unique crosslinks were detected. These were subsequently evaluated by calculating molecular distances between identified crosslinked residues using known crystal structures of homologous proteins.

Conversely, the results of the ATM *in vivo* crosslinking experiment were that, while informative crosslinks were not detected between ATM and other proteins, certain pathways were over-, and under-represented in the Co-IP of cells expressing the ATM constructs. Specifically, the parkin-ubiquitin proteasomal system pathway was over-represented, while the proteasome degradation pathway was *under*-represented. Additionally, the small heat shock protein 27 (Hsp27) was found to be enriched, a chaperone known for its protective role in protein aggregation diseases.

Table of Contents

List of Tables

List of Figures

List of Illustrations

INTRODUCTION

Ataxia telangiectasia (A–T), or Louis-Bar syndrome, is an inherited autosomal recessive disease caused by mutations in the ataxia telangiectasia mutated (ATM) gene. The canonical role of ATM is to maintain genome fidelity by facilitating repair following double-strand DNA breaks. ATM also plays a key role in redox control during oxidative stress. Loss of these two cellular functions is believed to underlie the source of A–T patients' physiological and neurological symptoms (1-3).

Cells with mutated ATM can undergo damage due to oxidative stress (4-6). ATM has been observed to form a covalent disulfide dimer following oxidative stress, and to phosphorylate substrates that inhibit cell growth and to activate autophagy via the mTORC1 pathway (7-9). ATM's inability to form a covalent dimer in response to oxidative damage may result in A–T patients losing sensory function in their neuronal cells (10). A specific separation-of-function, redox homeostasis-deficient ATM mutant has been found to result in the cell experiencing deficiencies in mitochondrial function and autophagy, leading to widespread protein aggregation (11).

While arsenite stress to cells normally initiates the cellular redox control pathway (12, 13), when ATM is mutated, ROS damage goes unchecked (14). The cellular response to ROS is one of the primary areas of investigation in this thesis.

When cells experience double-stranded DNA breaks due to exogenous sources (e.g. environmental factors such as ionizing radiation) or endogenous sources (e.g. free radicals formed through normal oxidative metabolism), a protective signaling cascade is mobilized (15). The Mre11-Rad50-Nbs1 (MRN) complex senses the damaged DNA, activating ATM, which phosphorylates DNA damage mediators (e.g. 53BP1, MDC1, BRCA1, H2AX) as well as downstream kinases (CHK2, p53), activating the cell cycle

checkpoint and arresting cell growth (14-20). If the extent of DNA damage is excessive, the apoptotic pathway is activated; otherwise DNA repair is initiated using either homologous recombination (HR) during the S and G_2 cell cycle phases, or through non-homologous end joining (NHEJ) (21).

The primary approach used for investigating protein interactions in this research was the DSSO cleavable crosslinking technique (22). Crosslinking proteins *in vivo* and *in vitro* enables one to infer which proteins were interacting at the time of the crosslinking reaction. Since DSSO cleavable crosslinking is still a relatively new protocol, the technique was first optimized using a purified MRN protein complex sample. Optimization of the crosslinking protocol and the evaluation of the MRN protein complex structure are the two other primary areas of investigation in this thesis.

Ataxia Telangiectasia Mutated and Oxidative Stress

Patients with ataxia telangiectasia (A–T) lack the normal ATM control of oxidative stress due to reactive oxygen species, resulting in the degeneration of cerebellar Purkinje cells (23-25). Neuronal cells are especially prone to oxidative stress-induced damage, in large part due to the the higher level of mitochondrial activity (26-29). Consequently, A–T patients undergo progressive neurodegeneration and suffer the effects of reduced cognitive function, and loss of coordination and fine motor control (30). As there currently is no established therapy for A–T (31), a better understanding of ATM dysfunction experienced by A–T patients may shed new insight into possible interventions for treating the effects of cellular damage due to oxidative stress.

Certain redox pathways are initiated due to oxidative stress, such as the Nrf2/Keap1 pathway (32), which serves both to initiate the expression of antioxidant genes (33) as well as to activate autophagy by up-regulating p62 (34). p53 is central to

another ROS-sensing pathway that promotes autophagy through the regulation of DRAM (35). ROS also result in the misfolding of proteins (36), which must be dealt with by the cellular 'protein quality control' system (37).

Misfolded proteins are primarily degraded by three pathways in mammalian cells: the ubiquitin proteasome system (UPS), macroautophagy and chaperone-mediated autophagy (CMA) (38-40). In the UPS pathway, slow-folding or misfolding proteins are recognized by ubiquitin ligases, which mark them for proteasome degradation (41). In macroautophagy, proteins are first assembled into aggresomes that are subsequently degraded by lysosomes (42). In CMA, misfolded proteins that display the consensus sequence KFERQ are recognized by chaperones and delivered directly to lysosomes for degradation. Aggregated proteins that are resistant to these three mechanisms can form inclusion bodies, or plaques, and can lead to neurodegenerative disease phenotypes (40).

The mechanism of protein aggregation and dysfunction in protein clearance in A–T is currently not well characterized, but it may resemble other protein aggregation and neurodegenerative diseases. While a mouse model of A–T did not result in a significant loss of atm -/- Purkinje cells, the neuronal cells reentered the cell cycle event (CCE), a process which can lead to neuronal cell death (43, 44). The ATM protein is also activated as a result of protein aggregation in Huntington's disease (HD), and the clinical phenotype of HD resembles A–T, including ataxia and cerebellar atrophy (45-48).

Research into these neurodegenerative diseases has characterized the cellular processes in which aggregated proteins are recognized and directed into the autophagy pathway. In Parkinson's disease (PD), parkin mediates lysine-63 (K63) linked polyubiquitination of misfolded proteins, triggering the retrograde transport of aggregated proteins to the nucleus to form Lewy bodies (27, 49). The proteins are then collected into an aggresome, followed by the assembly of an autophagic membrane, fusion to a

lysosome and degradation via autophagy. However, the role of ubiquitination is not fully understood in this process. In amyotrophic lateral sclerosis (ALS) disease, the Bcl-2-associated athanogene 3 (BAG3) – Hsp70 complex couples mutant superoxide dismutase (SOD) to the retrograde dynein motor to form Bunina bodies independent of an ubiquitination event (50-53).

Making use of the discovery that a disulfide-crosslinked ATM dimer is formed in response to oxidative stress (9), Paull, et al., created a separation-of-function ATM mutant (C2991L) that does not form this covalent dimer. Using it, they found that the cell cycle checkpoint was not activated following ROS treatment.

It was also confirmed that the adverse effects of the C2991L mutant on cell homeostasis extended to the mitochondria, in which membrane potential was lower, and levels of carnitine (and its derivatives) was higher due to deficiencies in mitochondrial function. Cellular compartment turnover was also affected, in that mitochondria were not effectively delivered to lysosomes for recycling via mitophagy, and other organelles were not properly recycled through autophagy. The investigations also found widespread protein aggregation in the C2991L mutants, especially upon arsenite treatment (11).

Research performed in our lab also revealed that heat shock proteins co-purify with ATM (2), so interactions between ATM and HSPs are of particular interest. The small heat shock protein 27 (Hsp27, also referred to as HSPB1) has been found to be highly expressed in the frontal cortex of A–T patient brains—conversely, the expression of other heat shock proteins, including Hsp70, is unchanged as compared to controls (54). Hsp27 is known for its protective role in the protein aggregation diseases HD, AD and ALS (55). Hsp27 is also known to function as a molecular chaperone of intermediate filaments (56). This suggests that Hsp27 might function similarly to HSPB8, which associates with the aggresome intermediate filaments vimentin, nestin and glial fibrillary

acidic protein (51). However, as other data indicates that BAG3 directs Hsp70 substrates to aggresomes (57), the specific mechanism of aggresome formation in ATM mutants is not clear—it could involve one, both or neither of these two heat shock proteins. Moreover, it's also not clear whether macroautophagy or CMA is the primary clearance pathway for misfolded and aggregated protein being used by ATM mutant cells.

Studies have also documented ATM mediated phosphorylation of heat shock proteins. ATM promotes Hsp27 phosphorylation in response to oxidative stress (58). In response to DNA damage, inducible heat shock proteins HSC70 (HSPA8), HSP72 (HSPA1A), Hsp90 and Hsp90α are phosphorylated to stimulate DNA repair (59-62). ATM also mediates phosphorylation of HSPB1 via TAO and the MAP kinase cascade (3).

During previous investigations with mouse models harboring kinase-dead ATM mutants, researchers noted that, while ATM null mice were viable, $Atm^{KD/KD}$ progeny were never produced, indicative of an embryonic lethal phenotype. Furthermore, they found that heterozygous kinase-dead/null ATM cells ($Atm^{KD/-}$) had greater genomic instability than ATM null cells ($Atm^{-/-}$) (63). This apparent oncogenic gain-of-function phenotype from a mutant tumor suppressor is not unlike that found with carcinogenic point-mutations found in p53 in atypical Li-Fraumeni Syndrome (LFS) (64). As ATM has critical roles in maintaining genomic stability (and is integrated with the p53 checkpoint pathway), these similarities might not be unexpected.

However, a detailed mechanism of the adverse ATM-kd cellular phenotype is not understood. A clue might be found in reviewing LFS-variant case studies in which the offending gene (or lack thereof) was not p53, but, rather, CHK2. In these cases, germline loss CHK2, or loss of (mutant-CHK2) heterozygosity resulted in the LFS phenotype (65). Since a loss of CHK2 results in unchecked Mdm2-mediated clearance of p53, genetic

instability and DNA damage accumulate, resulting in a multicancer phenotype (65, 66). In the same fashion, a kinase-dead ATM could both fail to initiate checkpoint arrest of cell growth due to a lack of kinase activity or because of irreversibly binding to a DDR tumor suppressor.

Latent accumulation of genetic damage can also account for the fact that mouse models and cell lines with homozygous null tumor suppressor genotypes (both ATM and p53) are initially viable, but inevitably result in a carcinogenic phenotype (63-68) or degraded cell viability (11).

Nevertheless, while the germline kinase deficient ATM mutants result in embryonic lethality in mice, temporally-expressed kd-ATM can still be a useful tool in studying ATM function in the cell. As was previously described, the kinase-deficient ATM mutant (kd-ATM) was found deficient in checkpoint activation following both CPT (camptothecin, DNA-damage inducing) as well as sodium arsenite treatment (11).

In the research described herein, to elucidate the substrate and binding partners of ATM in cells undergoing oxidative stress, both wild type and kinase-deficient ATM constructs were expressed in 293T cells and enabled co-IP enrichment using the FLAG tags. The kinase-deficient mutant ATM (kd-ATM) used in the investigations had two amino acid substitutions (D2886A and N2891K[1]) abolishing its ability to phosphorylate substrate[2] (11), but potentially also extending ATMs interaction time with its substrate, enhancing DSSO crosslinking.

[1] The residue numbers for the kinase-deficient sequences account for the two N-terminal tags.
[2] This mutant is unable to phosphorylate substrate in response either to DNA damage or oxidative stress.

The MRN Complex

The human MRN complex and homologous yeast Mre11-Rad50-Xrs2 (MRX) complex are critical to DNA double-strand break (DSB) repair in both mitosis and meiosis. The Mre11-Rad50-Xrs2/Nbs1 (MRX/N) complex has been shown to be involved in sister chromatid repair, homologous recombination (HR), non-homologous end joining (NHEJ), meiotic recombination, and telomere maintenance, participating in DNA repair during all phases of the cell cycle and during nuclear division of somatic cells as well as during meiosis (69-76).

Nbs1 gets its name from Nijmegen breakage syndrome (NBS), highlighting its role in maintaining genome stability. When there is a germ line mutation of Nbs1, cells undergo chromosomal breakage during replication and patients exhibit symptoms similar to A–T (77, 78). With certain Mre11 mutations, the DSB repair pathway is abrogated, resulting in an ataxia telangiectasia-like disorder (ATLD) (79). Both types of pathological mutations affect MRN complex interactions with ATM. Deficiencies in Rad50 can result in chromosomal instability, radiation hypersensitivity, predisposition to cancer and a phenotype similar to NBS in a disorder classified as Nijmegen breakage syndrome-like disorder (NBSLD) (80, 81).

Mre11 acts as a scaffold, in which a single His-to-Tyr amino acid substitution[3] abolishes formation of the MRX complex (70, 82). The N-terminal region of yeast Mre11 has also been shown to be necessary for homo- and hetero-dimerization, and the acidic heptad repeat near the C-terminus is important for full self-association (70, 71, 83). Evolutionarily-conserved Mre11 interacting regions (MIRs) also exist within both Rad50 and Nbs1 (81, 84-88). Within the human Nbs1 MIR is the NFKxFxK motif which,

[3] The substituted amino acid residue His213 in *Saccharomyces cerevisiae* is conserved residue His217 in *Homo sapiens* protein Mre11.

elucidated in a *S. pombe* crystal structure, revealed a surprising, asymmetrical association across the Mre11 dimer interface (81).

Through multiple sites of interaction, MRN recruits ATM following double-strand DNA breaks (16, 17, 89). Within the MRN complex, there are evolutionary-conserved regions required for ATM recruitment to damaged DNA. The C-terminus of Nbs1 contains an ATM-interaction motif (84, 87); and Rad50 in the Mre11/Rad50 (MR) complex recruits monomeric ATM to sites of DNA damage (16, 17).

Analysis of Protein Interactions using Crosslinking-Mass Spectrometry

In the DSSO cleavable crosslinking-mass spectrometry experiment, tandem spectra from crosslinked peptides are analyzed by the XlinkX algorithm developed by the Albert Heck Laboratory to elucidate protein binding partners *in vivo* (90, 91). In brief: proteins are crosslinked to their normal binding partners under experimental conditions, protein complexes of interest are enriched and analyzed using mass spectrometry.

To characterize the interactions ATM makes in cells undergoing oxidative stress, FLAG-tagged constructs of ATM were used to permit IP enrichment[4] (92). Cells were then incubated with oxidizing agents and, while cells were still responding to the stress, the proteins were crosslinked. The cells were then harvested, lysed and purified by immunoprecipitation. The purified protein complexes were then prepared for mass spectrometry analysis; they were reduced, alkylated and digested. The crosslinked peptides were then analyzed: peptides were chromatographically separated using a C18 reversed-phase column and analyzed using an Orbitrap Fusion hybrid mass spectrometer,

[4] The wild type (pATMwt-Flag) and kinase deficient plasmids (pATMkd-Flag) were gifts from Michael Kastan.

which contained the necessary firmware to perform the MS^n crosslinking instrument acquisition.

Mass spectrometry analysis of cleavable crosslinked peptides employed the MS^n method: (crosslinked) peptides eluting from the HPLC system, detected in the precursor (MS^1) scan, were isolated and fragmented with a low-energy collision-induced dissociation (CID) waveform (22). The low energy fragmentation generates two sets of characteristic peptide masses offset by the mass of the sulfoxide moiety from the cleavable DSSO linker (22)[5]. The instrument then sequentially isolates each of the peptides and fragments them with higher-energy collision dissociation (HCD), scanning out the individual peptide fragments in subsequent MS^3 scan events.

Acquired tandem spectra were then analyzed using the XlinkX algorithm included in the Proteome Discoverer 2.2 release of software. From the Orbitrap Fusion method editor, the 'Cleavable MS2-MS3' Peptides-Xlink MS acquisition template was used as a starting point, and incremental changes were made during method development to optimize detection of crosslinked peptides. The detection of crosslinked, highly-confident peptides infers that the two parent proteins were closely associated at the time of crosslinking. For the ATM analysis, ATM binding partners were co-precipitated with the FLAG-tagged ATM protein during IP purification step prior to sample preparation for mass spectrometry analysis.

[5] Gas-phase rearrangement during DSSO linker fragmentation results in dehydration such that the delta mass observed in the mass spectrometer is 31.97208 Da instead of the expected mass of sulfoxide.

MATERIALS AND METHODS

The materials and methods used in this research are described, below:

Tissue Culture

HEK 293T/17 cells (ATCC, CRL-11268) were grown (at 37 °C, 5% CO2, in humid incubator) in Dulbecco's Modified Eagle Medium (Fisher Scientific, 11995-073) supplemented with 10% fetal bovine serum (Gemini Bio-Products, 100-135)[6] and 1% Pen Strep (Fisher Scientific, 15140-122).

Protein Expression and Purification

MRN Complex Protein Sequences

Mre11 contains a linker sequence (LGA) followed by the FLAG tag (DYKDDDDK) at the C-terminus. Rad50 contains a linker sequence (PPAAAGG) at the location of the deleted coiled-coil domain, and the HA sequence (YPYDVPDYA) followed by a His-tag (HHHHHH) at the C-terminus. The coiled-coil domain deletion mutant of Rad50 was created using PCR amplification of the N-terminus (a.a. 1-216), the linker sequence, and the C-terminus (a.a. 1104-1312) of Rad50, as previously described (93). Nbs1 was the canonical sequence. The human MRN complex (hMRcdN) protein sequences are listed in the Appendix.

MRN Complex Expression and Purification

The human MRN complex proteins were expressed in *Sf*21 insect cells (Invitrogen, B82101) by co-expression using the Bac-to-Bac[7] baculovirus expression

[6] Chrysalis Insect Cell Qualified FBS was utilized for the purpose of depleting otherwise expiring stock.

[7] Mutant transfer vector pTP516 (Rad50cd), and wild type transfer vectors pTP813 (wt-Mre11) and pTP288 (wt-Nbs1) were converted into bacmids pTP542 (Rad50cd), pTP814 (wt-Mre11) and pTP291 (wt-Nbs1), which were then used to make the viruses according to the manufacturer's instructions.

vector system (Life Technologies) as previously described (85, 93-95). The *Spodoptera frugiperda* insect cells expressing the hMRcdN complex were lysed in Ni-NTA buffer (50 mM KH_2PO_4, 10% glycerol, 2.5 mM imidazole, 20 mM β-mercaptoethanol, 0.5 M KCl), homogenized and sonicated. The lysates were cleared using ultracentrifugation and loaded onto Ni-NTA agarose resin (QIAGEN). The proteins were washed, then eluted with Ni-B buffer (50 mM KH_2PO_4, 10% glycerol, 250 mM imidazole, 20 mM β-mercaptoethanol, 50 mM KCl). The eluate was then loaded onto 1 mL of anti-FLAG M2 affinity resin (Sigma, A2220-2), washed with Buffer A (25 mM Tris pH 8.0, 100 mM NaCl, 10% glycerol, 1 mM DTT) and eluted with 0.1 mg/mL of FLAG peptide (Sigma) in Buffer A. The peak fractions were loaded onto and eluted from a Superose 6 column (GE Healthcare) equilibrated with a modified MOPS buffer (25 mM MOPS pH 7.0, 100 mM NaCl, 2% glycerol, 1 mM DTT), which enabled crosslinking later without quenching of the DSSO crosslinker reagent. The aliquots from the peak fractions were flash frozen and stored at -80°C until use (85).

ATM CONSTRUCT PROTEIN SEQUENCES

The wild type (pATMwt-Flag) and kinase deficient plasmids (pATMkd-Flag) were gifts from Michael Kastan (92). Both the wild type and kinase-deficient ATM sequences include a FLAG tag (DYKDDDDK) followed by a His-tag (HHHHHH) at the N-terminus. The kinase deficient sequence contains two additional mutations, D2886A and N2891K[8]. Since the detection of the FLAG peptide was skewing the ATM quan results, the N-terminal FLAG sequence was omitted from the FASTA file for Proteome Discoverer searching of proteins binding to the ATM constructs. Additionally, since the sequenced plasmid contained two additional amino acid substitutions that were

[8] The residue numbers for the kinase-deficient sequences account for the two N-terminal tags.

contradicted by the mass spec analysis, those were also omitted and the canonical sequences were instead used for data analysis.

ATM Construct Expression

Calcium phosphate transfection was used to induce ATM expression in the 293T cells, as previously described (89, 92).

ROS Treatment of Cells

HEK 293T/17 (293T) cells were grown to 80% confluency on 15-cm plates in 20 mL of media, to which was added 10 µL of 50 mM AsO3 solution for a final As(III) concentration of 25 µM, and incubated over-night for 18 hours. Cells were then harvested.

Cell Harvesting

Forty-eight 150-mm plates of each experimental condition of 293T cells were harvested in the biohazard hood using ice-cold PBS (with 25 µM AsO_3 to continue the ROS treatment until just before crosslinking) using physical agitation and a gentle stream of solution to dislodge the cells. Cells were collected into 15 mL Falcon tubes (four plates per tube), which were kept on ice until crosslinking. Falcon tubes were centrifuged at 4 °C, 100×g to concentrate cells during triple PBS rinses.

Protein Crosslinking

Proteins were crosslinked using the DSSO (disuccinimidyl sulfoxide) reagent (Thermo Scientific, A33545)[9] according to the vendor's recommendations. The MRN

[9] Publication number MAN0016303 Revision A.0.

complex proteins were crosslinked using the *in vitro* protocol, and the ATM proteins were crosslinked using the *in vivo* protocol. Details of the crosslinking protocols follow:

IN VITRO MRN COMPLEX CROSSLINKING

Purified 20-µL aliquots of ~300 nM MRN complex protein samples in 25 mM MOPS, 100 mM NaCl and 2% glycerol were removed from 80 °C freezer and thawed on ice. DSSO reagent was removed from 4 °C refrigerator and warmed to room temperature. DSSO reagent was reconstituted by adding 51.5 µL of DMSO to make 50 mM stock solution. 42 µL of DSSO stock solution was added to the MRN complex aliquot (42 µL of DMSO was added to the control), for target 300:1 linker to protein ratio, and was gently vortexed to mix. The sample – reagent solution was permitted to incubate for 60 minutes at room temperature, then the reaction was quenched by adding 1.25 µL of 1 M Tris buffer, pH 8.0. Crosslinked proteins were then reduced, alkylated and digested using the FASP protocol.

IN VIVO ATM CELL CROSSLINKING

Fifty-mL Falcon tubes of harvested cells, on ice, were rinsed with ice-cold PBS to remove AsO_3 solution. DSSO reagent was removed from 4 °C refrigerator and warmed to room temperature. Each 1 mg vial of DSSO reagent was reconstituted by adding 51.5 µL of DMSO to make 50 mM stock solution. 463.5 µL of ice cold PBS was added to each 51.5 µL stock of 50 mM DSSO to make the final 5 mM DSSO crosslinking solution. Using the Tecan Spark Multimode Microplate Reader, cell count was estimated to be approximately 2.8×10^9 per treatment sample—far exceeding the target of 10^7 cells—so four vials of DSSO reagent were used to crosslink each sample of harvested cells. Excess PBS was removed from the cells, then 2.06 mL of 5 mM DSSO crosslinking solution was added to each cell sample and vortexed to mix (the same amount of DMSO was added to

the control). The sample–reagent solution was permitted to incubate in ice for 30 minutes. The reaction was then quenched by adding 20 μL of 1 M Tris buffer, pH 8.0, and permitted to incubate on ice for 15 minutes. Excess Tris–PBS solution was removed from the cells, the cells were then flash frozen and stored at -80 °C until they were ready for FLAG-tag immunoprecipitation.

Sample Preparation

The samples were prepared for mass spectrometry analysis, from both the *in vitro* crosslinked MRN complex and *in vivo* crosslinked ATM proteins, using the following protocols:

FLAG-tag Immunoprecipitation (Co-IP)

FLAG-tag immunoprecipitation was used to extract ATM and its crosslinked clients, as previously described (89, 96). FLAG-tag enriched proteins were then reduced, alkylated and digested using the FASP protocol.

Filter-Aided Sample Preparation (FASP)

Crosslinked samples were prepared for mass spectrometry analysis using a modified version of the Filter-Aided Sample Preparation (FASP) method described by Wisniewski *et al.* (97), taking special care to prevent filter leakage during filtering steps (98). In brief, Microcon-30kDa centrifugal filters (EMD Millipore, MRCF0R030) are first prewashed by adding 400 μL of a rinse solution (20% ACN, 2% formic acid) and centrifugal spinning at 10,000 × g[10]. The samples are then diluted 5:1 with UA solution (8M urea in Tris buffer, pH 8.8), added to the filters and centrifuged. The samples are then rinsed twice with 400 μL of UA solution and the proteins are reduced by incubating

[10] Reduced centrifuge speeds were used to prevent filter breakage during filtering steps

with 400 µL of 50 mM dithiothreitol in UA (Fisher Scientific, BP172-5) for five minutes. The filter cartridges are again centrifuged and the proteins are alkylated with 400 µL of 50 mM iodoacetamide (Sigma-Aldrich, I1149-5G) for five minutes. The filter cartridges are centrifuged, and then rinsed twice with 400 µL of 40 mM ammonium bicarbonate, pH 7.8 (Fisher Scientific, A643-500)[11].

PROTEIN DIGESTION

The reduced and alkylated proteins were digested on filter using several different enzymes to produce peptides of different lengths and amino acid composition in order to increase protein coverage during subsequent analysis. In each case, 0.5 µg of enzyme was dissolved in 100 µL of 40 mM ammonium bicarbonate buffer, the solution was added directly to the centrifugal filters, the filter devices were closed and vortexed to mix, and then placed in a sample box with moistened towels and incubated overnight at 37 °C.

The following mass spectrometry grade enzymes were used to digest the protein samples: GluC V-8 endoproteinase (New England Biolabs, P8100S), Trypsin Gold (Promega, V5280), chymotrypsin (Roche, 11418467001), and LysN protease (Pierce, 90300).

PEPTIDE DESALTING

Following protein digest, samples were eluted with 20% ACN, 2% formic acid, evaporated to dryness (Eppendorf Vacufuge 5301 Concentrator), resuspended with with 0.5% LC-MS grade TFA (Thermo Scientific, 85183), then desalted using the DigestPro MSi robotic sample preparation instrument (INTAVIS Bioanalytical Instruments).

[11] For samples to later be digested with GluC endoproteinase, the final FASP rinses were instead performed with NEB GluC reaction buffer.

XL-MS Data Acquisition and Analysis

Data was acquired with the Orbitrap Fusion Tribrid mass spectrometer, using scan parameters defined in the standard Peptides-Xlink cleavable MS2–MS3 template, with the following modifications: MS^2 charge state filter included charges 2–15 as well as undetermined charge states, MS^2 intensity threshold was 5.0×e3 and The MS^3 charge state filter was removed.[12]

Data was analyzed using the DSSO_MS2_MS3.pdAnalysis default Proteome Discover 2.2 template, with the following notable changes: Semi-enzymatic specificity was used instead of the default 'full' setting (specific enzyme selected based upon digest performed for actual sample). A minimum peptide length setting of 3 was used instead of 5 for the XlinkX search node. Additional dynamic modifications included deamidation (of asparagine), dehydration (of serine and threonine), a delta mass of +12.000 Da (on the peptide N-terminus[13]) and methionine loss/acetylation (at the protein N-terminus).

To perform an independent evaluation of crosslinked spectra, a Scan Event Filter node was connected to the Spectrum Selector to pass MS^3 spectra (only) directly to another Sequest HT[14] node, using the same search parameters as the XlinkX search node, plus additional dynamic DSSO alkene and thiol fragment modifications[15].

Protein Homology, Pathway and Structural Analysis

Once crosslinks were determined from the acquired data, the interacting regions were evaluated further using the following software tools:

---

[12] Even with this reduced intensity threshold value, some crosslinked peptide intensities fell beneath this value, not triggering an MS3 acquisition, ultimately resulting in a lowered crosslink spectrum match score.
[13] Artefacts suggested by Preview™ by Protein Metrics, Inc. © 2011-2017.
[14] SEQUEST® is used by Proteome Discoverer under license from the University of Washington.
[15] DSSO alkene fragment formula: C(3)OH(2); DSSO thiol fragment formula: C(3)OSH(2).

PROTEIN CROSSLINK VISUALIZATION

Following computational analysis of the mass spectrometry data of crosslinked proteins, a fasta file of the proteins and a CSV file of the crosslinks were exported from Proteome Discoverer. An additional CSV file was manually created to annotate the protein domains, and all three files were uploaded to the xiNET cross-link viewer at http://crosslinkviewer.org/ (99). Wild type proteins, which contain canonical sequences and are described in the fasta file using the standard UniProtKB accession, can be automatically annotated in the online viewer with the UniProt and SuperFamily domains (100-102).

PATHWAY OVER-REPRESENTATION ANALYSIS

Pathway over-representation analysis was performed by uploading the accessions of enriched proteins to the Thermo Scientific pathway over-representation cloud application at https://apps.thermofisher.com/apps/lsms/pa/#/. The June 2016, Revision B of the web application uses pathway information from the WikiPathways, KEGG (Kyoto Encyclopedia of Genes and Genomes) and Reactome Pathway database repositories.[16]

SEQUENCE HOMOLOGY SEARCHES

Protein BLAST searches were performed on the NCBI BLASTp website https://blast.ncbi.nlm.nih.gov/Blast.cgi?PROGRAM=blastp&PAGE_TYPE=BlastSearch&LINK_LOC=blasthome (103).

Sequence homology searches were also performed with available structures on the Research Collaboratory for Structural Bioinformatics (RCSB) Protein Data Bank (PDB) to at https://www.rcsb.org/pdb/home/home.do#Subcategory-search_sequences (104).

---

[16] WikiPathways content is provided under the Creative Commons CC BY-NC-SA 3.0 License. KEGG is a Copyright © of Pathway Solutions Inc. and Kanehisa Laboratories. Reactome is a Copyright © of Cold Spring Harbor Laboratory and the content is provided under the Creative Commons Attribution 4.0 International License.

Evaluation of evolutionarily conserved sequences was performed using the T-Coffee algorithm at http://tcoffee.vital-it.ch/apps/tcoffee/do:regular (105, 106).

STRUCTURAL VISUALIZATION AND MEASUREMENTS

Protein complex visualization and molecular measurements were performed with the PyMOL Molecular Graphics System, Version 2.0.1 Schrödinger, LLC (107).

RESULTS AND DISCUSSION

A discussion of the results of this research are described, below:

DSSO Crosslinking

DSSO crosslinking was performed on purified MRN complex proteins, with and without additional nucleotides (ATP), proteins (ATM) and cofactors ($MgCl_2$). Crosslinking was also performed on sets of 48 15-cm plates of 293T cells expressing the different ATM constructs (wild type, and kinase-dead), which were treated for 18 hours with 25 μM AsO_3. The following sections describe the modifications made to the standard protocols suggested by the mass spectrometry equipment and reagent manufacturer:

OPTIMIZING CHEMICAL CROSSLINKING PROTOCOL

The DSSO reagent was titrated into the purified MRN complex sample targeting the manufacturer's recommended range of 20–400 fold molar excess of crosslinker-to-protein complex concentration (see Illustration 1, below). In agreement with the manufacturer's protocol, while crosslink reporter peaks were found with DSSO concentrations below the 20× molar excess, no crosslinks could be confidently identified by the XlinkX algorithm. When crosslinking the ATM construct-expressing cells, a recommended final crosslinker concentration of 5 mM of DSSO was used; although significantly more cells were treated at once than the 10^7 cells specified in the protocol.

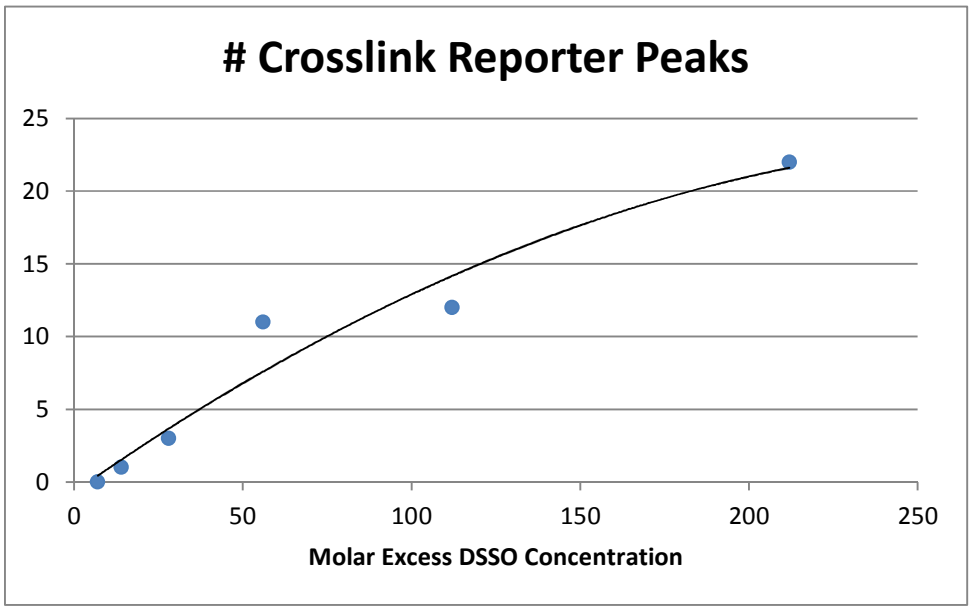

Illustration 1 Number of crosslinks found with DSSO concentration

In the following sections, the significance and relevancy of the detected crosslinks is discussed, but, in general, the following principles were taken in consideration: Both inter- and intra-protein crosslinks were compared with the currently-known protein structures to determine whether they were in agreement with known dimensions and atomic distances. The crosslinks were also evaluated based upon whether they were detected reproducibly, and if its XlinkX score was above the 1% FDR threshold using the Percolator validation method (90, 108)[17]. The reagent and protein concentrations for each experiment were controlled to keep as much as possible within the manufacturer's recommendations to reduce non-specific protein-protein interactions.

[17] In the event that there are not enough crosslink spectrum match candidates, the Percolator validation approach may fail, in which event the Xlinkx validator reverts to target-decoy FDR validation.

ALTERNATIVE ENZYME DIGESTION APPROACHES

Digestion with trypsin yielded the most number of identifiable crosslinks from the DSSO crosslinking experiments. Of the 53 crosslinks detected in the experiments, 41 were found using trypsin as the digesting enzyme. Even more revealing, of the 115 detected peptides linked by DSSO, 81 contained an arginine residue at the C-terminus, while only three had lysine at the C-terminus—indicating that the DSSO crosslinker inhibited trypsin hydrolysis of peptide bonds adjacent to lysine.

A small percentage (5%) of the crosslinked peptides were cleaved at the N-terminus of a crosslinked lysine residue, which suggested that the LysN enzyme (Peptidyl-Lys metalloendopeptidase) might give complementary results to trypsin. However, due to the higher-frequency of missed cleavages (up to 5 missed cleavages per individual peptide), the peptides were much larger (up to 29 a.a. residues per crosslinked peptide), had multiple crosslinks and/or linker fragments and were uninterpretable by the XlinkX algorithm—in fact, no crosslinks were successfully identified, despite an otherwise high percentage of crosslink reporter peaks detected in the MS^2 spectra.

The rest of the crosslinks detected in the experiment were from either the chymotrypsin or GluC digestion, resulting in ten and two additional crosslinks, respectively. Even more discouragingly, only one of the crosslinks was an inter-crosslink between different proteins within the complex, and it received the lowest XlinkX score (7.60) of all the crosslinks detected. The major drawback of these alternative enzymes was the much lower likelihood that the peptides contained basic residues in their amino acid sequence, and were thus not carrying a positive charge so that they could be detected in the mass spectrometer.

Optimizing XL-MS Data Acquisition

A couple important changes were made to the default crosslinking acquisition template to enable additional crosslinked peptides to be detected by the mass spectrometer and subsequently processed by the software algorithms. Specifically, the precursor ions included for MS^2 fragmentation and further mass spectrometric analysis was modified from the default of 4–8 charge state to include ions with charge states as low as +2.

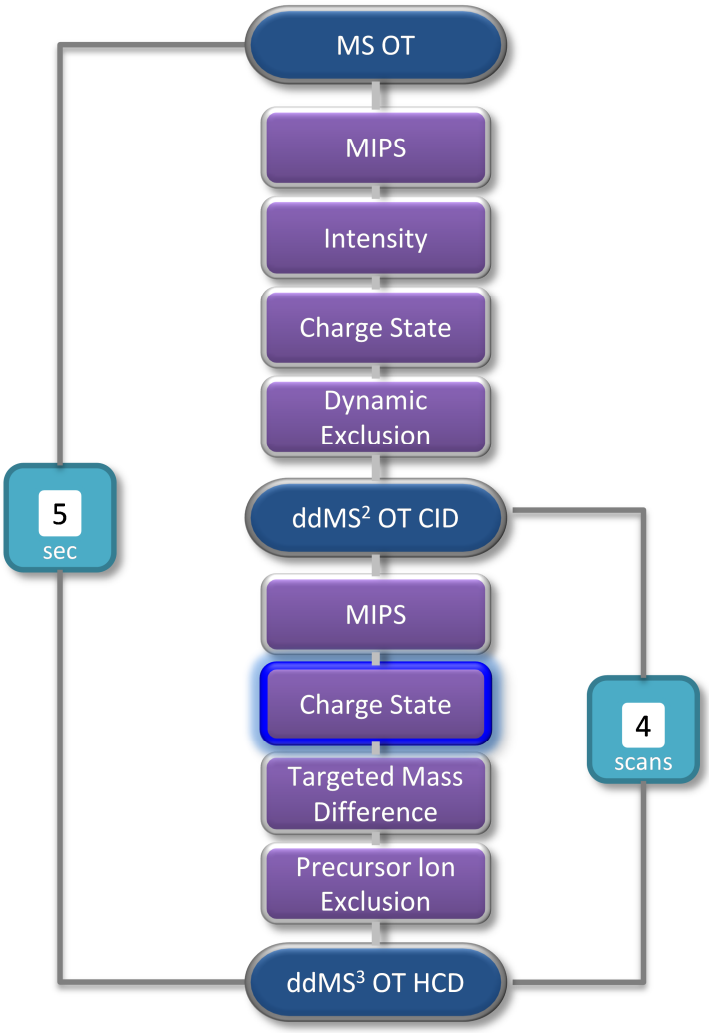

Illustration 2 *Default Orbitrap Fusion peptides-Xlink acquisition template with removed MS^3 charge state filter node highlighted blue.*

These changes permitted the analysis of peptides cleaved by alternative enzymes that did not cleave at basic residues (which, consequently, have lower charge states due to the peptides having a lower frequency of lysine and arginine residues).

Additionally, the charge state filter for MS^3 fragmentation was removed to permit the inclusion of singly-charged peptides, as was the case for most of the GluC-digested MRN crosslinks and half of the chymotrypsin-digested crosslinked peptides (Illustration 2 , above).

OPTIMIZING DATA PROCESSING

To account for incomplete enzymatic digestion, a 'semi' enzymatic specificity was used in the search algorithm. To ensure that smaller peptides were detected by the XlinkX search node, the minimum peptide length was reduced from 5 to 3. Smaller peptides were generated during GluC and Chymotrypsin digestions, but the shorter peptide lengths still did not produce ambiguous crosslinks[18], as defined by the xiNET cross-link viewer (99). Common post-translational modifications were added to the default search parameters, such as dehydration of serine and threonine and loss of methionine/acetylation of the protein N-terminus. To account for chemical artefacts produced during sample preparation, additional dynamic modifications (deamidation of asparagine and +12 delta mass of peptide N-terminus[19]) were also included. Finally, the hydrolyzed DSSO modification of lysine was also added to the XlinkX search node to include peptides that contained dead-end crosslinking modifications.

[18] Ambiguous crosslink data results from (especially short) amino acid sequences that are found more than once within a single protein or in more than one protein.
[19] Artefacts suggested by Preview™ by Protein Metrics, Inc. © 2011-2017.

Without these additional dynamic modifications, several redundant crosslink spectrum matches would be missed, but only one unique, low scoring crosslink[20] would not have been identified, so the increased complexity of the search parameters is not entirely necessary to analyze the mass spectrometry data.

Evaluating Crosslinking Results

Fifty-three unique crosslinks were found within and between the MRN complex proteins, and each crosslink was identified an average of two times (see Figure 1, below).

Most crosslinks were identified in at least two replications for the particular enzyme preparation (unique crosslinks were typically only identified in a single type of digest, due to the different cleavage specificities of the enzymes). The most reproducible crosslinks were also found in multiple charge states (e.g. +3 and +4) in each replicate. times and from the different replicates. The most reproducible crosslinks were also assigned much higher XlinkX crosslink scores. For example, the intra-crosslink between residues 510 and 609 of Mre11 was found in multiple charge states in the five trypsin digests, and in ten separate sets of mass spec scans (the crosslink peptide pairs were detected in 10 separate MS^2 spectra, and the individual peptides were confirmed by an additional 36 MS^3 scans). The range of XlinkX scores for this unique crosslink was between 55.57 and 345.85.

[20] Crosslink assigned a low score due one of the crosslinked peptide pairs not being confirmed with tandem MS^3 spectrum due to ion current beneath the specified intensity threshold in the acquisition method.

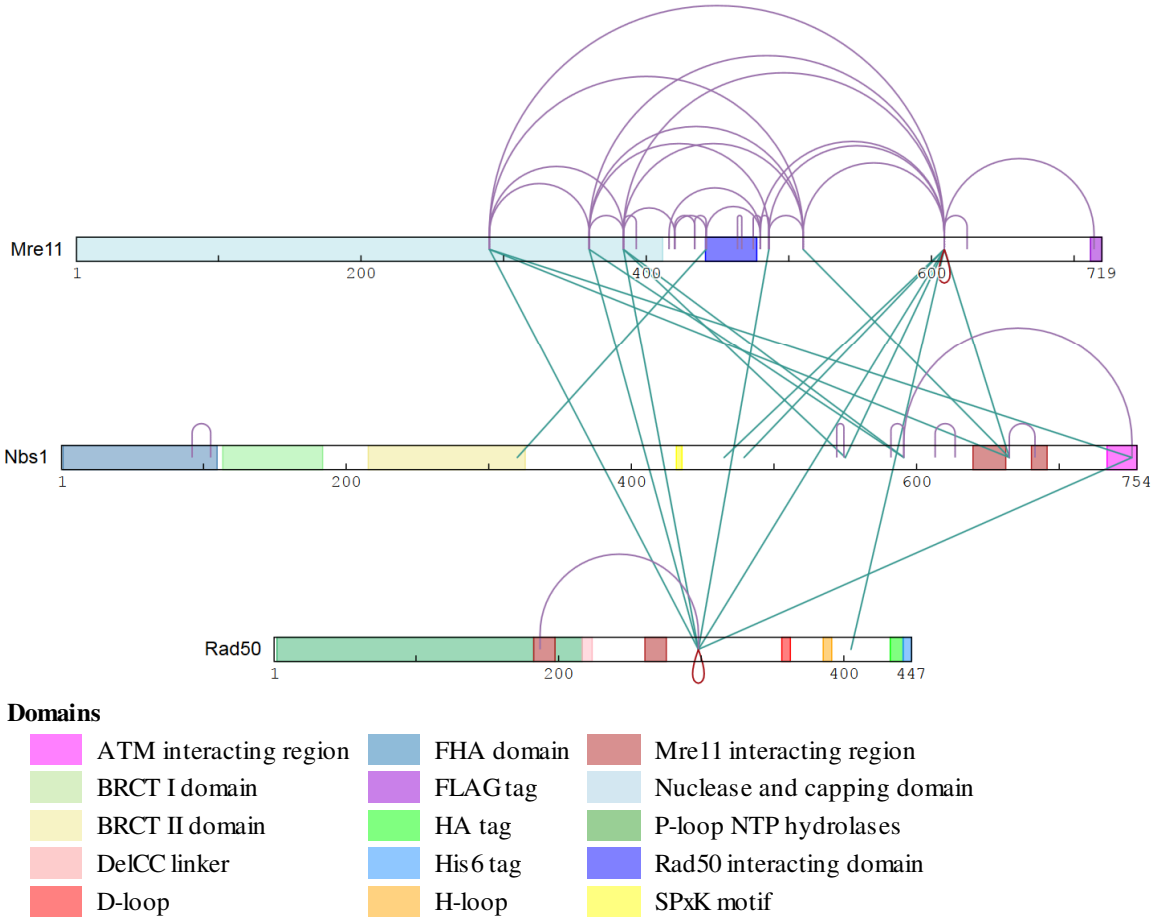

Figure 1 Fifty-three unique crosslinks detected in the MRN complex with the coiled-coil domain of Rad50 deleted (99)[21].

At the other end of the continuum were crosslinks that were found only once, from a single sample replicate, and/or with a low XlinkX score. As an example, the crosslink identified between residue 320 on Nbs1 and 442 on Mre11 was found only once, being assigned the lowest XlinkX score from the data set (7.60) and with only one of the peptides being 'confirmed' with a unique MS^3 spectrum (and with an improbable number of modifications—four). For the purpose of evaluating the likelihood of this later

[21] The interactive image can be viewed at:
http://crosslinkviewer.org/uploaded.php?uid=45fc37ae346f0222d6c89fd06c0afcd8335b2985

crosslink, the candidate can safely be eliminated. The rest of the identified crosslinks fell somewhere between these two extremes, and require a somewhat more critical assessment.

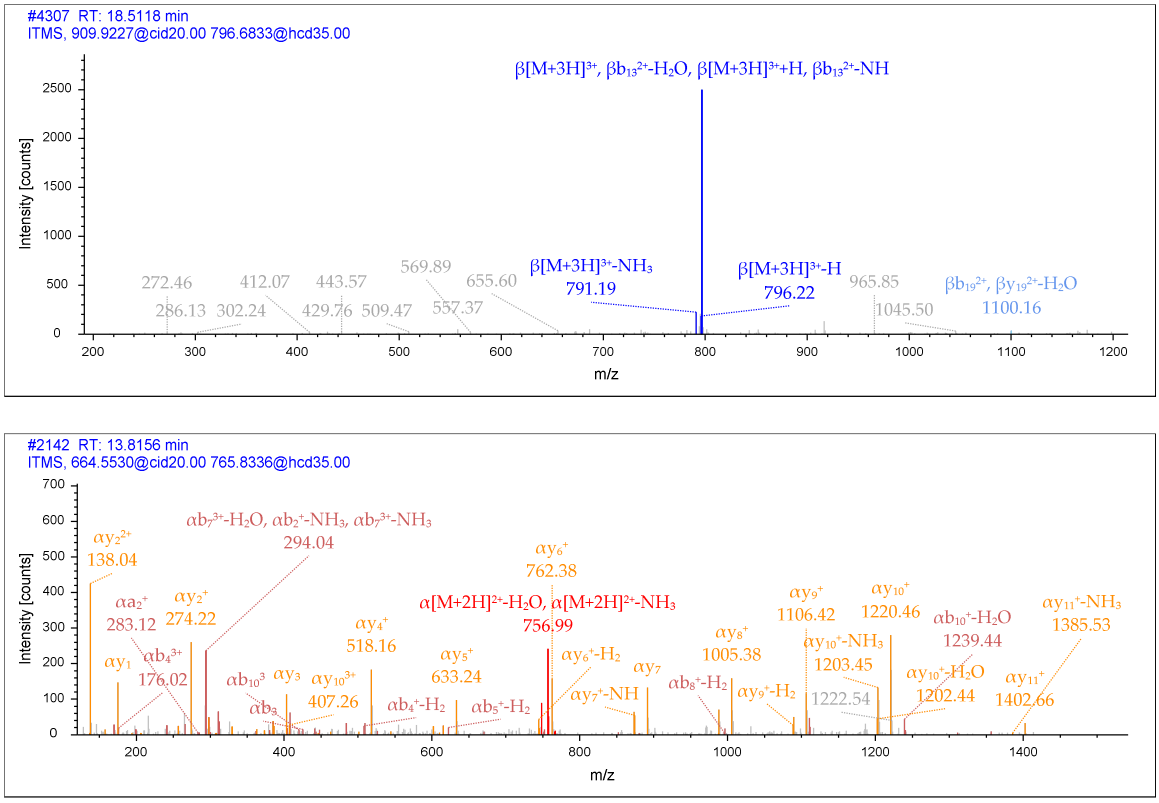

Figure 2 Visual comparison of MS^3 spectra of crosslinked peptides contrasting low-, to high-sequence coverage (90, 91).

For a first approximation, the quality of the crosslink spectrum matches (CSMs) for the best scoring crosslink (between residues 510 and 609 of Mre11, discussed above) could be used to assess the quality of the other crosslinks identified. Since the lowest scoring CSM for this crosslink had an XlinkX score of 55.57, and was also confirmed with four complementary MS^3 spectra (properly detecting both DSSO fragments for each peptide), these quality metrics were used as a baseline for determining which of the other

crosslinks to spend additional time evaluating. Two general approaches were used to assess the other crosslinks: spectral quality and structural analysis.

The spectra were evaluated based upon the assigned XlinkX score, by whether an independent search of the same spectra using a different searching algorithm (in this case, Sequest HT[22]) and whether a visual inspection confirmed that most of the predominant ions in the spectrum were accounted for by the 'expected' peptide fragments following HCD fragmentation. Analysis of the crosslinks based upon known, solved protein structures is discussed further in the next section.

Structural Analysis of MRN Complex

While evidence has shown that the N-terminal region of yeast Mre11 is necessary for dimerization (71), in DSSO crosslinking of the human MRN complex, the N-domain of Mre11 did not produce any crosslinks (Figure 1). From studies of the crystal structure of a human Mre11 dimer, it was observed that the dimerization buried a large surface area of the Mre11 core (1850 Å), which might have contributed to the inability of the DSSO reagent to access this region (88). As depicted in Figure 3, below, the two closest lysine residues between the Mre11 molecules were 16.2 Å apart (K66:K105). In the mass spec data, both the alkene and thiol DSSO fragments were detected by the XlinkX algorithm at Lys-66, but the DSSO moiety at Lys-105 was hydrolyzed[23], perhaps due to the somewhat unstructured nature of the molecule at that location, preventing crosslinking.

[22] SEQUEST® is used by Proteome Discoverer under license from the University of Washington.
[23] Hydrolyzed DSSO modification at Lys-105 detected by the Sequest HT node.

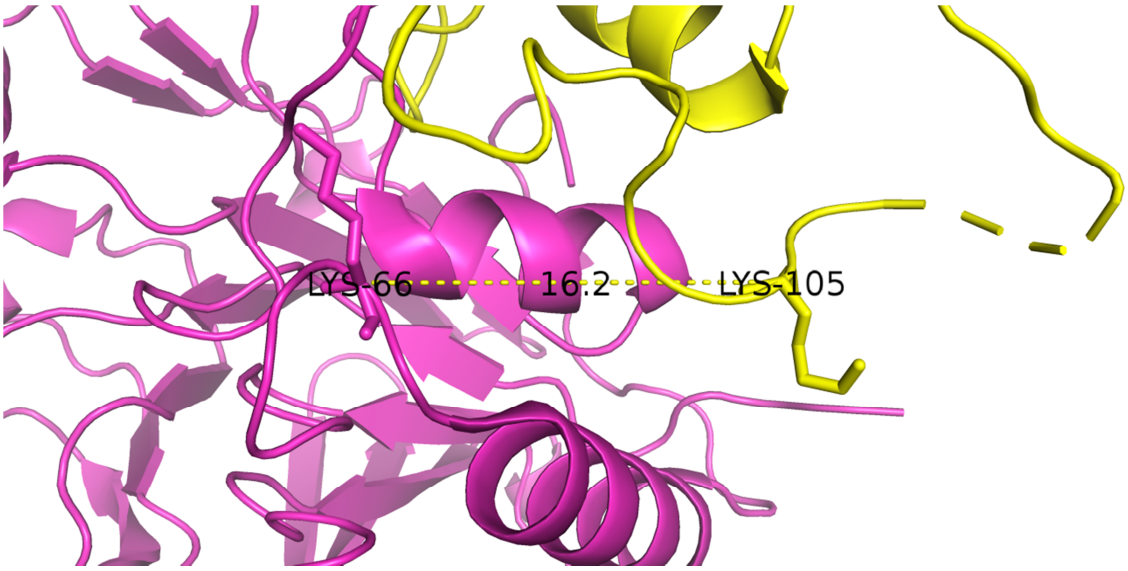

Figure 3 Distance between nearest Mre11 dimer lysine residues was 16.2 Å. Image of PDB structure 3T1I created with PyMOL (88, 107).

Another region in yeast Mre11, near the C-terminus, contains an acidic heptad repeat that was shown to be important for self-association (71, 83), and while a moderately homologous region exists on human Mre11 (BLASTp score of 13.9, E-value of 1.1, 30% identity), this putatively homologous region did not converge with a detected Mre11 intra-crosslink (Figure 1). The conserved Mre11 His217 residue, corresponding to the amino acid residue His213 in Saccharomyces cerevisiae, which, when substituted with tyrosine abolishes MRX complex formation, is not located near any detected crosslinks.

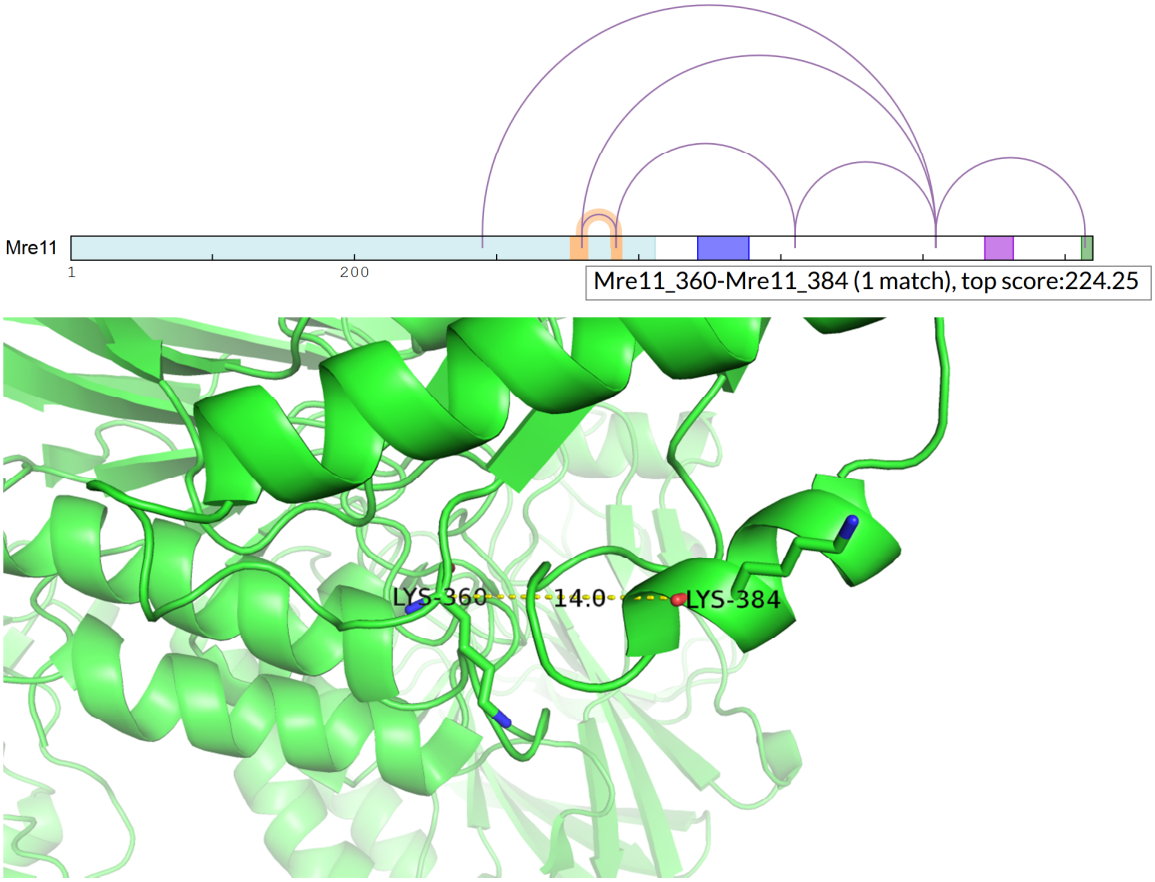

Figure 4 Intra-crosslink detected by mass spectrometry within Mre11 confirmed by PDB structure 3T1I created with PyMOL (88, 99, 107).

Three other semi-conserved residues[24] within the *M. jannaschii* Mre11:Mre11 interface that, when mutated (i.e. Met65Arg, Glu94Ala, Leu99Trp), abolishes Mre11 dimerization, also did not overlap with DSSO crosslinked regions (109). However, while the *P. furiosus* residue, Leu-97 (which, when mutated, abolished the dimerization of Mre11) did have a homologous human residue (Ala-331) that was near the crosslinked Lys-360 residue (27.1 Å), the region did not correspond to an interacting region in the

[24] Homologous human residues adjacent to the *M. jannaschii* residues Met-65 and Leu-99 were conserved, and three residues up-to and including the *M. jannaschii* residue Glu-94 was conserved (human Glu-411).

human Mre11 PDB crystal structure 3T1I (88). However, this might be accounted for by the fact that the MRN complex exists in (at least) two distinct conformational states (93).

Another observation was that one significant Mre11 intra-protein crosslink (matched three times with XlinkX scores between 127 and 229) was between the highly reactive Lys-609 residue and the FLAG-tag residue Lys-714 (see Figure 1). The proximity of the FLAG-tag being so close to a region of Mre11 that also associates with Nbs1 and Rad50 suggests that the tag may either compete or interfere with the normal quaternary structure of the MRN complex.

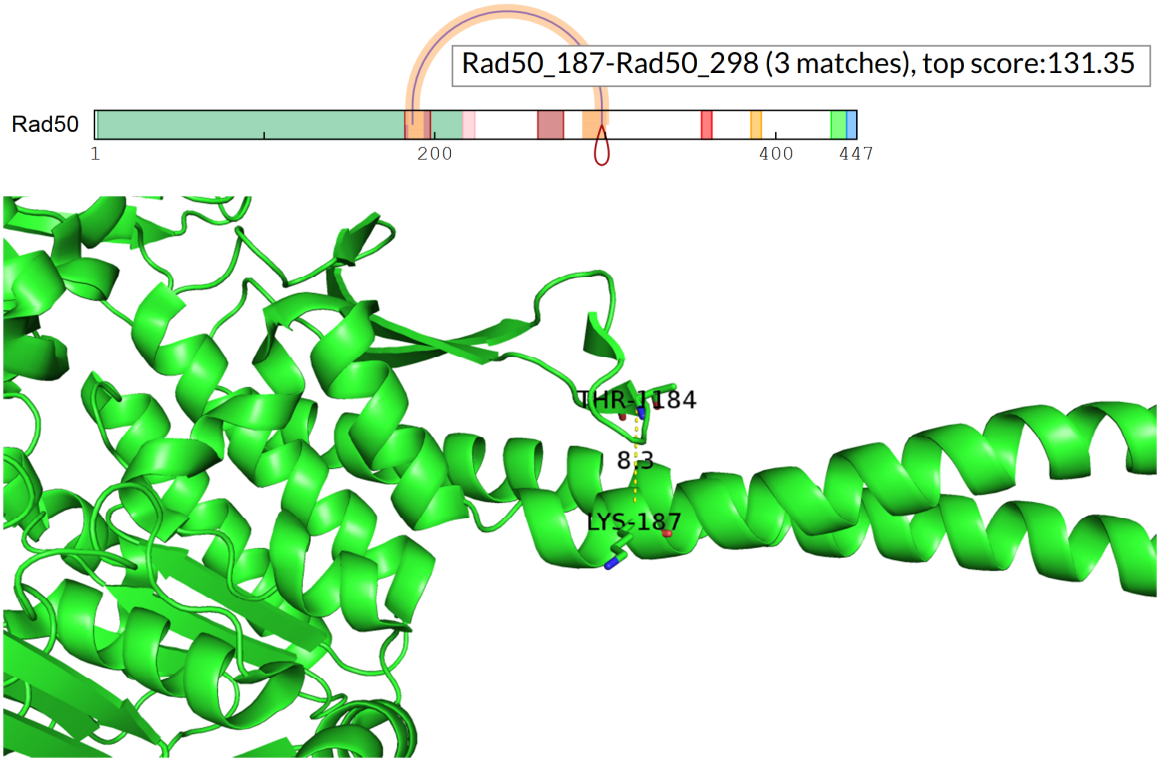

Figure 5 Intra-crosslink detected by mass spectrometry within Rad50 evaluated with PyMOL using homologous *C. thermophilum* PDB structure 5DAC (99, 107, 110).

While there currently is not a solved crystallography structure of the human MRN complex, there are a few structures of individual proteins or of regions of interaction

between proteins within the complex, but not necessarily from human samples. There is a tetrameric crystal structure of the N-terminus (up to a.a. 400) of human Mre11 (88). The extent of the structure does permit evaluation of a particularly-high XlinkX scored inter-protein link (224.25) within Mre11 detected by mass spectrometry between the Lys-360 and Lys-384 residues. The distance measured between the α-carbons of the two lysine residues in PyMOL was 14.0 Å (see Figure 4, above), well within the 23.4 Å maximum distance constraint of the DSSO cross-linker (90).

Two Rad50 lysine residues shown to be crosslinked by mass spectrometry were evaluated by measuring the distance between the analogous residues in homologous *C. thermophilum* PDB structure 5DAC (110). The measurement of 8.3 Å was especially impressive given the fact that the two α-carbons are separated by nearly 1,000 amino acid residues in the wild type protein (see Figure 5, above).

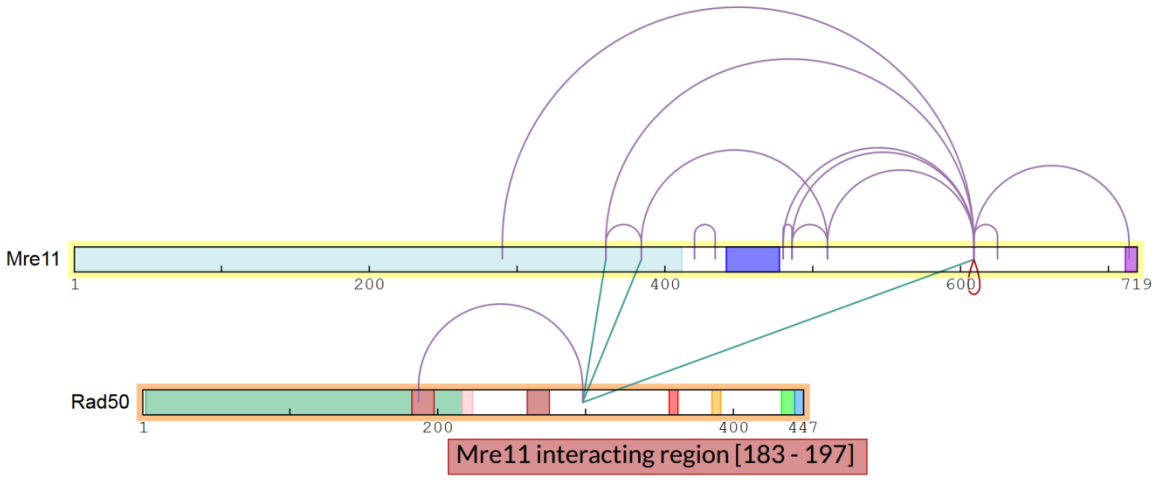

Figure 6 Crosslinks at the Mre11 interacting region in Rad50 and between Rad50 and Mre11 (99).

The close spatial proximity of the two Rad50 lysine residues described above suggests that the previously annotated Mre11 interacting region (MIR) on Rad50 (111) is

responsible for the distal lysine inter-protein crosslinks between Rad50 and Mre11 (Figure 6, above).

Also in support of previously annotated Mre11 interacting regions on Nbs1 (81, 85), using an XlinkX cutoff score of 100, three interlinks were detected between Mre11 and Nbs1 (see Figure 7, below).

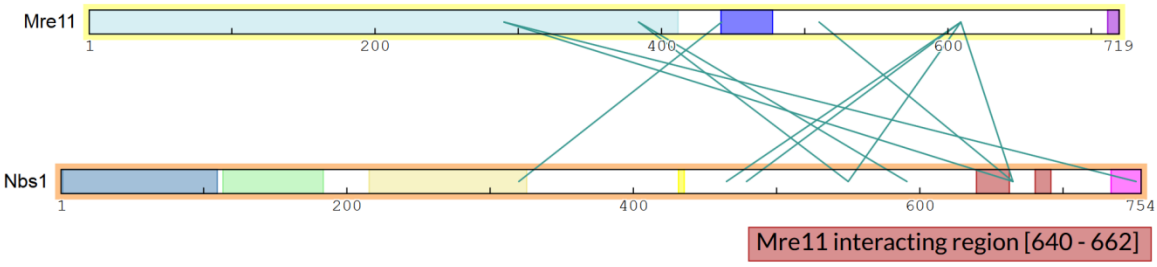

Figure 7 Inter-crosslinks at Mre11 interacting region in Nbs1 between Nbs1 and Mre11 (99).

Since the human Mre11-Nbs1 complex structure has yet to be solved, the crosslinks between these proteins had to be evaluated using similar structures. To do so, a dimer from the human Mre11 tetramer PDB structure 3T1I was aligned with a homologous *S. pombe* Mre11 dimer from the Mre11-Nbs1 PDB structure 4FBW, enabling a visualization of the proximity of the Mre11 Lys-290 residue to the Nbs1 peptide, which contains the Mre11 interacting region (MIR) (81, 88, 107). Despite the fact that homologous lysine residue does not exist in the *S. pombe* structure, it is nevertheless apparent that the human Lys-290 detected in the mass spectrometry crosslinking experiment aligns perfectly with the Nbs1 MIR (see Figure 8, below). The non-conserved *S. pombe* Ser-504 residue, which aligns with the human Lys-665 residue,

would be the last residue just upstream of the Nbs1 fragment (MIR region), but is missing from the 4FBW crystal structure (Figure 8) (81).

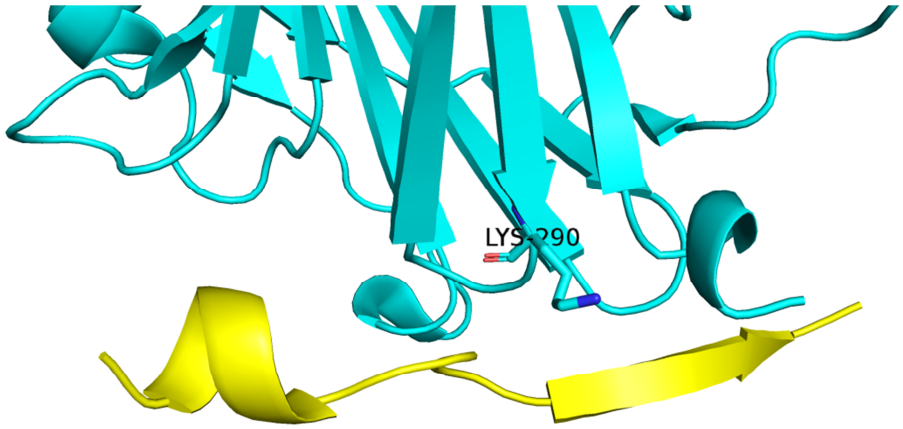

Figure 8 Evaluation of Nbs1 MIR crosslink to Mre11 using PyMOL alignment of human Mre11 PDB structure 3T1I with homologous *S. pombe* Mre11-Nbs1 PDB structure 4FBW (81, 88, 107).

While other previously-annotated interaction regions, such as the Rad50 interacting region on the C-terminus of Nbs1 (81), were also corroborated with the mass spectrometry crosslinking experiment, we wanted to know whether any of the other 'hot spots'[25] included evolutionarily-conserved regions. While a sequence comparison performed on T-Coffee did not reveal any conserved regions, surprisingly, the K290 residue on Mre11 was conserved on the five species surveyed: *H. sapiens*, *A. fulgidus*, *C. elegans*, *C. cinerea* and *A. thaliana* (see Figure 9, below).

Lys-384 on Mre11, the second hot spot, is within a short, seven-amino acid α-helix located between two otherwise unstructured turns (Figure 4), likely imparting its ability to interact both with Rad50 and Nbs1. The third hot spot, Lys-609 of Mre11, is

[25] A hot spot hereby being defined as an amino acid residue found to make three or more interactions with one or more other proteins within the MRN complex.

located in the center of a region[26] from a splice variant found only in isoform 1 of Mre11. Gene ontology annotation results from a UniProtKB peptide search[27] of this region included the protein C-terminus binding molecular function, which suggests that this region might be important for protein-protein interactions.

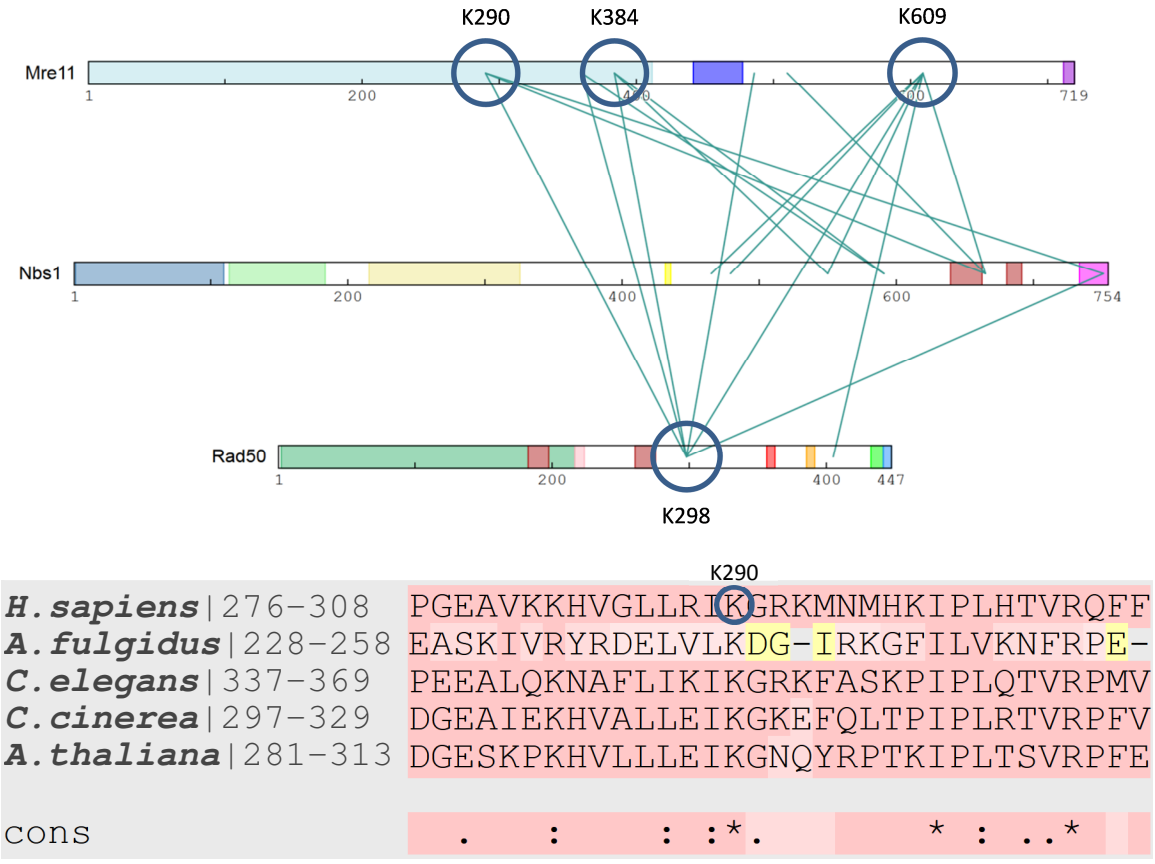

Figure 9 Mre11 'hot spot' Lys-290 found to be evolutionarily conserved by comparing multiple species using the T-Coffee algorithm (105, 106)[28]. Accessions compared: P49959=*H. sapiens*, O29231=*A. fulgidus*, Q23255=*C. elegans*, Q9UVN9=*C. cinerea* and Q9XGM2=*A. thaliana*.

[26] a.a. variable splicing sequence ADTGLETSTRSRNSKTAVSASRNMSIID, annotated by NCBI at: https://www.ncbi.nlm.nih.gov/protein/P49959.3?report=genbank

[27] Peptide search performed at: http://www.uniprot.org/peptidesearch/

[28] Sequence alignment performed at: http://tcoffee.vital-it.ch/apps/tcoffee/do:regular

Lys-298 of Rad50, the final hot spot, is located within the P-loop superfamily region of the protein. In the *C. thermophilum* crystal structure, the analogous residue (Thr-1184) is located in an unstructured turn of the protein (Figure 5). As such, the flexibility of the region most likely accounts for the six crosslinks that were found with the other proteins in the complex.

MRN Protein Complex Purity

During analysis of the mass spectrometry data, the crosslinked peptides were searched against the canonical protein sequences to enable visualization of the automatic UniProtKB and SuperFamily annotations from the crosslink viewer website. This revealed a very low scoring crosslink (XlinkX score of 6.85) between Mre11 and the Rad50 coiled-coil zinc hook domain—a portion of the protein sequence that was deleted from the expressed protein. While the Rad50 peptide was clearly incorrect, its erroneous identification still suggested that unexpected crosslinks to contaminants might be occurring.

To perform a more comprehensive search for peptide candidates, the data was analyzed using the much larger UniProtKB/Swiss-Prot fasta database[29] (112). Unexpectedly, a tobacco hornworm heat shock protein was identified with 15 unique peptides—unprecedented for a typical contaminant besides the enzyme(s) used during digestion. In fact, only Mre11, Rad50 and Nbs1 were identified with more peptides, as would be expected.

Since the *Sf*21 insect cell expression system used to clone the MRN complex proteins originates from *Spodoptera frugiperda*, the presence of a moth heat shock protein should not have been a surprise (85, 113). Performing the same contaminant

[29] There were 467k protein sequences in the 4/5/2017 release of the Swiss-Prot fasta database.

search, this time using a smaller fasta file from just the *Ditrysia* (moths, butterfly) clade, revealed the presence of three additional moth heat shock proteins, one of which was identified with 41 unique peptides (see Figure 10, below). Fortunately, while the presence of moth HSPs was confirmed, no crosslinks were detected between the MRN complex proteins and the contaminants.

Accession	Description	Contaminant	Marked as	Sum PEP Score	# Unique Peptides
Nbs1	(O60934) NBN_HUMAN Nibrin OS=Homo sapiens GN=NBN PE=1 SV=1			1659.884	330
Mre11	(P49959) MRE11_HUMAN Double-strand break repair protein MRE11 OS=Homo sapiens			1611.865	340
Rad50	(Q92878) RAD50_HUMAN DNA repair protein RAD50 OS=Homo sapiens GN=RAD50 PE			558.444	154
305693941	70 kDa heat shock protein [OS=Spodoptera litura]			154.482	41
P00766	Chymotrypsinogen A OS=Bos taurus PE=1 SV=1	X		87.472	27
P0C1U8	Glutamyl endopeptidase OS=Staphylococcus aureus GN=sspA PE=1 SV=1	X		75.288	24
27260894	heat shock cognate 70 protein [OS=Spodoptera frugiperda]			48.559	14
P00761	Trypsin OS=Sus scrofa PE=1 SV=1	X		32.872	5
223036830	Heat shock protein 70 [OS=Spodoptera exigua]			27.665	12
12005809	90 kDa heat shock protein HSP83 [OS=Spodoptera frugiperda]			26.569	10
P81054	Peptidyl-Lys metalloendopeptidase OS=Grifola frondosa GN=MEP PE=1 SV=2	X		25.940	4

Figure 10 Four moth HSP contaminants in the MRN complex sample (marked green) in addition to the four enzymes (orange).

FUTURE DIRECTIONS

The hot spots identified in the crosslinking experiments should be further investigated by mutating specific residues, such as Lys-290 in Mre11 (Figure 9), or by deleting small regions, such as the seven-amino acid α-helix that encompasses Lys-384 in Mre11 (Figure 4), to determine if MRN interactions are abolished.

ATM Response to Oxidative Stress

To confirm protein aggregation in U2OS cells with ATM inhibited using KU-55933 (EMD Millipore, 118500), the detergent-insoluble fraction of cell lysates was isolated and analyzed by mass spectrometry using standard protocols previously described (114). As expected, the insoluble fraction contained the intermediate filaments

which form the cytoskeleton of aggresomes, vimentin and nestin, and were significantly enriched[30] in the ATM inhibited cells (see Figure 11, below) (115).

Also from the analysis of the aggresomal proteins, multiple protein clearance pathways were enriched, as expected. Proteins were enriched that are implicated in multiple protein aggregation diseases (Alzheimer's disease, Huntington's disease and Parkinson's disease), such as the mitochondrial ubiquinone, cytochrome and ATP synthase complex proteins. Other enriched pathways included the parkin-ubiquitin proteasomal system pathway (WP2359), Pink/Parkin Mediated Mitophagy (R-HSA-5205685), the unfolded protein response (UPR) pathway (R-HSA-381119), E3 ubiquitin ligase pathway (R-HSA-8866654) and other ubiquitination and chaperone pathways…

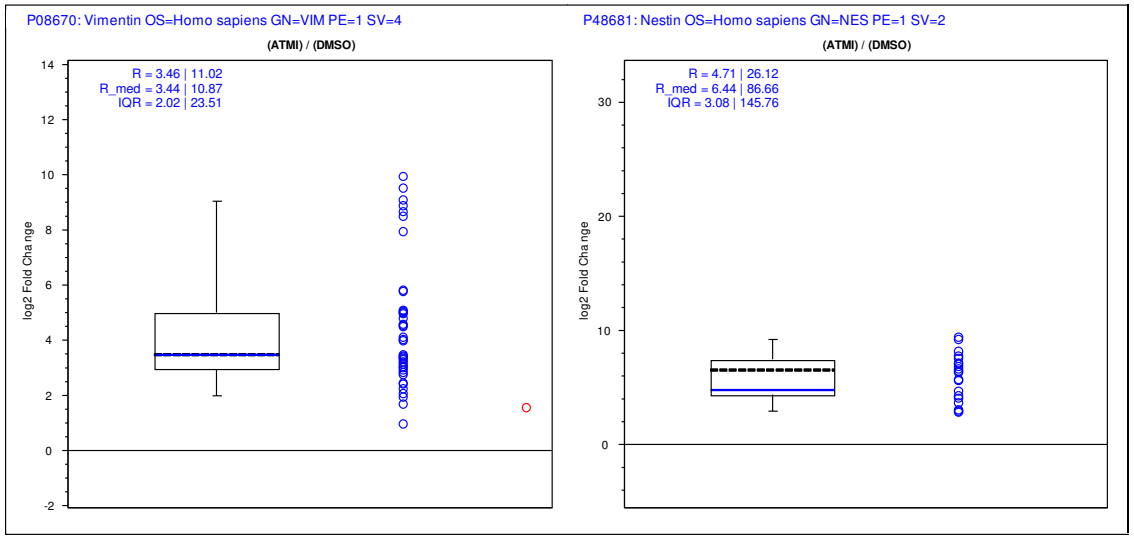

Figure 11 Intermediate filaments highly enriched in isolated aggresomes

As might also have been expected, since aggresomal proteins were being analyzed, was that the proteasome degradation pathway (WP183) was *under*-represented.

[30] Significance of protein enrichment determined using ANOVA (with respect to background protein populations of the two conditions) in which the Benjamini-Hochberg adjusted *p* value less than 0.001.

What was not expected was the magnitude of the under-representation of the WP183 pathway proteins in the ATM-inhibited sample—the FDR-adjusted *p* value (116) was $5.8\times e^{-32}$—especially since many other E3 ligase and molecular chaperones were present in the aggresome.

In the search for a more definitive understanding of the protein-degradation pathology in cells undergoing oxidative stress, we endeavored to enrich proteins that interacted directly with ATM in cells by crosslinking the cellular proteins *in vivo*. To this end, constructs of the ATM proteins (wild-type and kinase dead)[31] were transiently transfected into HEK-293T cells with concurrent arsenite exposure to induce oxidative stress, the proteins were crosslinked in cells using DSSO, and the ATM proteins were purified using a standard co-immunoprecipitation (co-IP) protocol (96).

Unlike the *in vitro* DSSO crosslinking experiments using the purified MRN complex proteins, high-quality informative crosslinks were not detected between ATM and other proteins.[32] The low level of ATM relative to the other proteins present in the cells were likely the primary reason for this, as even overexpressed ATM is not highly expressed. Also, despite using four vials of DSSO reagent per sample of harvested cells, this amount of reagent was still less than target reagent-to-cell count recommended by the protocol. Regardless, approximately 100 proteins were found exclusively in the IP of the cells expressing one of the ATM constructs and another 200 proteins were enriched at least two-fold.

Pathway analysis of these proteins found again that the parkin-ubiquitin proteasomal system pathway (WP2359) was over-represented, suggesting that ATM may

---

[31] The wild type (pATMwt-Flag) and kinase deficient (pATMkd-Flag) plasmids were gifts from Michael Kastan.

[32] Individual MS^3 spectra confirmed ATM crosslinks, but the only protein crosslinks detected by the XlinkX algorithm were within and between the high abundant, non-specifically enriched proteins.

participate in protein clearance utilizing parkin-mediated, K63-linked polyubiquitination of misfolded proteins, triggering the aggregation of proteins to form perinuclear inclusion bodies (aggresomes) (53).

The ATM *in vivo* DSSO crosslinking also did not appear to enrich many heat shock proteins, with the exception of HSPB1 (also called Hsp27), which was ~27% enriched in the cells expressing the wild type ATM construct, and ~70% enriched in the cells expressing the kinase-deficient ATM construct. This result is of particular interest because the small heat shock protein 27 has been found to be highly expressed in the frontal cortex of A–T patient brains, and is known for its protective role in the protein aggregation diseases, including ALS (54, 55). Moreover, studies have previously documented that ATM promotes Hsp27 phosphorylation in response to oxidative stress, so enrichment of this protein would be expected (58).

Accession	Gene Symbol	Description	Exp. q-valu	Score Sequest	# Peptides	Coverage [%]	Marked as
Q3ZCM7	TUBB8	tubulin beta-8 chain [OS=Homo sapiens]	0.000	93.23	12	30%	
Q13315	ATM	Serine-protein kinase ATM [OS=Homo sapiens]	0.000	87.67	28	11%	
P10412	HIST1H1E	Histone H1.4 [OS=Homo sapiens]	0.000	81.98	15	42%	
Q16576-1	RBBP7	Histone-binding protein RBBP7 [OS=Homo sapiens]	0.000	59.83	8	28%	
Q9UJW0-1	DCTN4	Dynactin subunit 4 [OS=Homo sapiens]	0.002	11.93	2	9%	
P0C0S5	H2AFZ	Histone H2A.Z [OS=Homo sapiens]	0.002	11.69	3	23%	

Figure 12 Co-precipitation proteins in stress pathway with ATM (R-HSA-2262752, marked orange in report).

From the group of proteins not detected in the controls, several of them shared with ATM the same cellular 'stress response' pathway (R-HSA-2262752) (see Figure 12, above). Being such a general pathway, it did not reveal a specific mechanism of interaction between the proteins. The unifying theme was the modification of histones (or histone variants). Otherwise, the features that tie these proteins together are that they

predominately reside in the nucleus, and that they bind and/or have catalytic activity for DNA, nucleotides or proteins.

An overly-simplistic interaction mechanism would be for ATM to phosphorylate H2A.Z to affect transcriptional repression, but the histone does not contain the expected [ST]-Q motif near the C-terminus (as is the case with H2A.X, which is phosphorylated by ATM during DNA repair) (117). Instead, it contains an SQ sequence near the N-terminus, at the beginning of the p-family (PF00125) H2AF core domain. Moreover, the three detected peptides (six peptide spectrum matches) did not provide adequate protein coverage to discriminate between two possible protein candidates, H2A.Z and H2A.V, which differ in sequence by only three amino acid residues (not at the SQ location), so this piece of the puzzle could not be satisfactorily reconciled with this data set[33].

A more compelling mechanism would instead involve the other histone in this protein set—H1.4—in which the main components in the pathway might be: ROS → ATM → p53 → H1.4 → repressed transcription (118-120). Moreover, p53 was enriched 2.5:1 in the wt-ATM sample and 1.7:1 in the kd-ATM sample. Alternatively, it might involve the histone binding protein (RBBP7), in an interaction mechanism such as: ROS → ATM → ? → RBBP7 → HDAC1/2 → H2A → repressed transcription.

Performing pathway analysis on the proteins that were at least two-fold enriched, no proteins remained in the proteasome degradation pathway (WP183). This resulted in an under-representation pathway with an FDR-adjusted *p* value score of $5\times e^{-4}$ and would seem to reinforce the observation that ATM's role in protein clearance during oxidative stress is not the direct mobilization of the proteasome. This was also in agreement with the results of the analysis of the previous data set from the aggresomal proteins. The other

[33] This data was acquired with a 40-minute acquisition—the data acquired from a 180-minute separation was also inconclusive.

significant, relevant over-represented pathways are listed in Table 1, below, and in the Appendix.

Pathways	Count	Raw p-value	FDR p-value
Cellular responses to stress	12	4.10E-10	1.24E-07
PRC2 methylates histones and DNA	6	3.02E-09	2.29E-07
Cellular Senescence	8	1.50E-08	5.69E-07
Epigenetic regulation of gene expression	7	3.58E-08	1.20E-06
Oxidative Stress Induced Senescence	6	2.65E-07	4.88E-06
PKMTs methylate histone lysines	5	2.74E-07	4.88E-06
HDACs deacetylate histones	5	8.48E-07	1.17E-05
DNA methylation	4	3.32E-06	3.86E-05
Cell Cycle	10	4.32E-06	4.67E-05
Nonhomologous End-Joining (NHEJ)	4	1.59E-05	1.42E-04
G2/M DNA damage checkpoint	4	7.22E-05	4.97E-04
Recruitment and ATM-mediated phosphorylation of repair and signaling proteins at DNA double strand breaks	3	6.51E-04	3.29E-03
DNA Double Strand Break Response	3	6.82E-04	3.33E-03
DNA Damage/Telomere Stress Induced Senescence	3	7.14E-04	3.44E-03
DNA Double-Strand Break Repair	4	7.71E-04	3.64E-03
Processing of DNA double-strand break ends	3	1.57E-03	6.62E-03
ATM Signaling Network in Development and Disease	3	6.87E-04	1.08E-02
NF-kappa B signaling pathway	3	2.45E-03	2.74E-02

Table 1 Over-represented pathways in enriched ATM IP samples

Acc. Key	*Description*	*Gene*
Q8IW41	MAP kinase-activated protein kinase 5	MAPKAPK5
P68431	Histone H3.1	HIST1H3F
P62805	histone H4	HIST1H4A
Q71DI3	Histone H3	HIST2H3A
P84243	histone H3.3	H3F3A
Q16576-1	Histone-binding protein RBBP7	RBBP7

Table 2 Oxidative Stress Induced Senescence pathway (R-HSA-1640170)

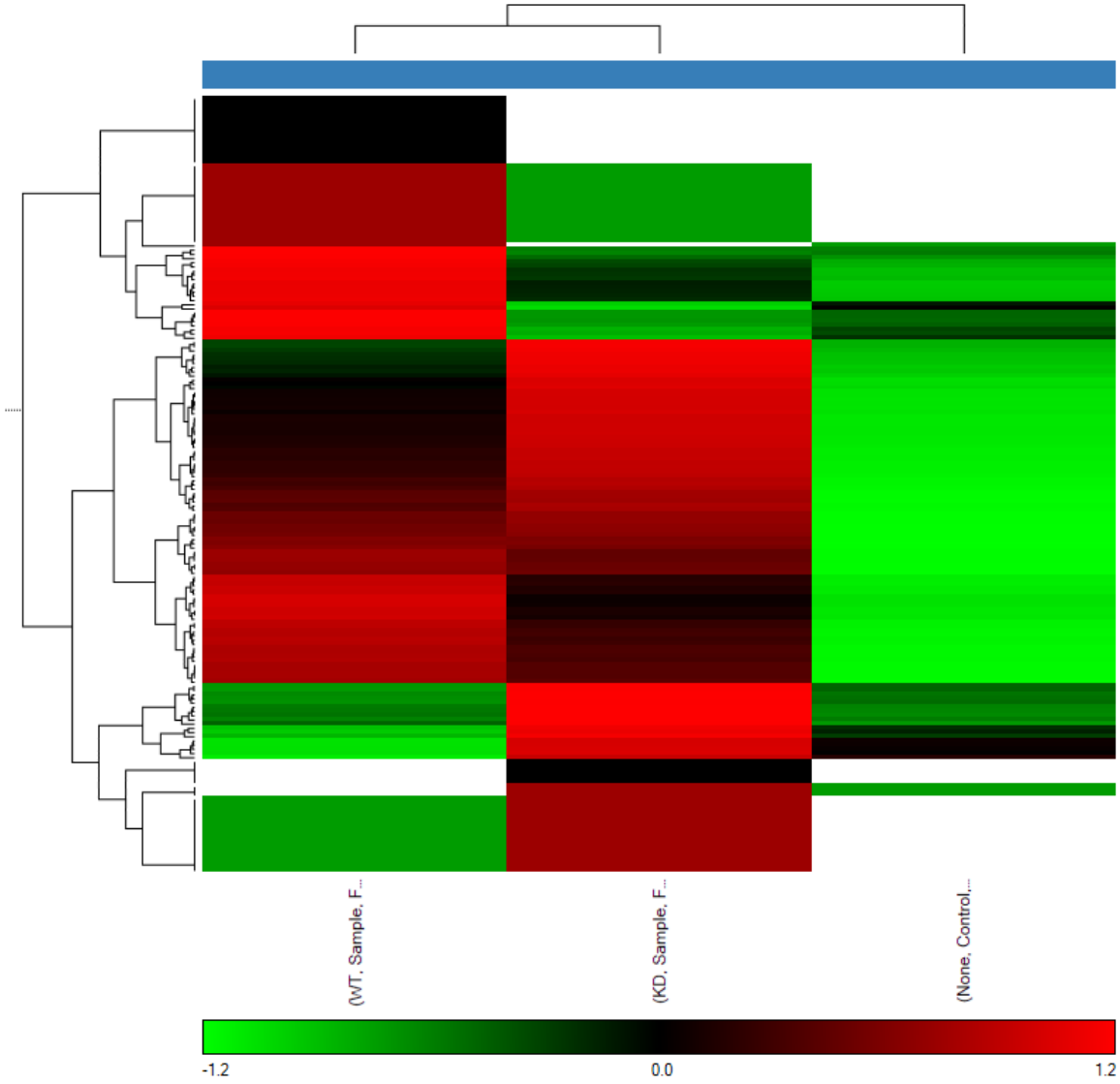

Figure 13 Cluster of proteins highly enriched in cells expressing ATM grouped by abundances. Key: Red = enriched, Green = depleted, White = not found, Black = quantified or parity fold change.

Lastly, when clustering the identified proteins based upon abundances (see Figure 13, above), and evaluating pathway over-representation, the oxidative stress induced senescence pathway (R-HSA-1640170) was identified with an FDR-adjusted *p* value

score of $1\times e^{-3}$, reinforcing the finding that oxidative homeostasis was affected by the treatment with sodium arsenite (see Table 2, above).

This filtering also elucidated an additional, highly-enriched protein with a Sequest score higher than ATM an abundance ratio-adjusted *p* value score of $4.2\times e^{-4}$: Leucine-rich PPR motif-containing protein (P42704, LRP 130). LRP 130 binds single-stranded DNA (ssDNA binding inferred from electronic annotation, gene ontology accession[34] GO:0003697), participates in a p53 regulatory pathway (R-HSA-5628897) and is a potential interacting partner of Parkin (121).

Additional protein sequence coverage was achieved from a 3-hour acquisition, one particular protein stood out that had a higher Sequest score than ATM—isoform 2 of drebrin (Q16643-2, DBN1). A deficiency of drebrin has been linked to cognitive decline in Alzheimer's patients, which is of particular interest since it, too, is a protein aggregation disease (122).

The unique C-terminal peptide for this isoform of the protein was identified by Sequest only in the kinase-dead ATM sample, with a Percolator *p* value score of less than $1.0\times e^{-4}$ (Percolator PEP score of $2.40\times e^{-5}$, Percolator SVM score of 0.772) (123). Conversely, the canonical version of the protein (Q16643) contained a peptide with a phosphorylated serine (Ser-601) that was found only in the wild-type ATM sample (ptmRS site probability of 90.96%). The phosphorylated serine residue is within an SQ motif[35,36], as is consistent with expected kinase substrates for ATM, therefore warranting further investigation.

---

[34] Copyright © 1999-2017 the Gene Ontology (CC-BY 4.0)

[35] The ptmRS validated, phosphorylated residue has also previously been independently verified, and is annotated by UniProt.

[36] Unexpectedly, the STQ motif was also duplicated, in succession: SQpSQ, a.a. 659 – 662.

FUTURE DIRECTIONS

Another set of controls should be created to evaluate the binding partners of ATM when the cell is not stressed with AsO3 treatment to differentiate the role of ATM in oxidative homeostasis. Additionally, to reduce non-specific binding of proteins during IP enrichment, magnetic beads could be used for the FLAG-tag enrichment step, or the co-IP enrichment could instead use His-tag affinity beads. Lastly, since the kinase activity of ATM is of central concern, alternative separation and purification techniques should be explored in order to enrich phosphopeptides, such as strong cation exchange/IMAC enrichment (124, 125).

CONCLUDING REMARKS

ALTERNATIVE CROSSLINKING APPROACHES

Crosslinking-mass spectrometry using cleavable crosslinkers is a relatively new protocol, and will likely require further optimization. Specifically, while the DSSO crosslinking reagent is cell membrane permeable, it is so at a relatively low efficiency (91). As such, alternative crosslinking reagents that more easily permeate the cell membrane, such as Disuccinimidyl Dibutyric Urea (DSBU), may prove more amenable to studying *in vivo* ATM interactions (126, 127).

Additionally, different crosslinker lengths or other classes of crosslinking reagents could be used which target different amino acid residues, for instance using sulfhydryl or carboxylic acid, instead of amine-reactive, NHS ester chemistry (128-130).

Lastly, protein complexes could instead be studied in wild-type cells using trifunctional crosslinking reagents. In this alternative approach, enrichment of protein complexes is performed with reactive group covalently attached to the crosslinker (such as biotin) instead of using tags expressed on cloned proteins (129).

AUTHOR DISCLOSURE STATEMENT

The author is an employee of Thermo Fisher Scientific, manufacturer of the Orbitrap Fusion Tribrid mass spectrometer and Proteome Discoverer software.

Appendix

OVER-REPRESENTED PATHWAYS

The following is a selection of the pathways that were over-represented in the FLAG-tag IP enriched ATM sample data:

Cell Cycle

Acc. Key	*Description*	*Gene*
Q13315	Serine-protein kinase ATM	ATM
P84243	histone H3.3	H3F3A
P68431	Histone H3.1	HIST1H3F
P62805	histone H4	HIST1H4A
Q71DI3	Histone H3	HIST2H3A
Q16695	histone H3.1t	HIST3H3
Q09028	Histone-binding protein RBBP4	RBBP4
Q16576-1	Histone-binding protein RBBP7	RBBP7
Q9Y230	RuvB-like 2	RUVBL2
P61981	14-3-3 protein gamma	YWHAG

Table 3 Cell Cycle pathway (R-HSA-1640170)

Cellular Senescence

Acc. Key	*Description*	*Gene*
Q13315	Serine-protein kinase ATM	ATM
P84243	histone H3.3	H3F3A
P68431	Histone H3.1	HIST1H3F
P62805	histone H4	HIST1H4A
Q71DI3	Histone H3	HIST2H3A
Q16695	histone H3.1t	HIST3H3
Q09028	Histone-binding protein RBBP4	RBBP4
Q16576-1	Histone-binding protein RBBP7	RBBP7

Table 4 Cellular Senescence pathway (R-HSA-2559583)

Nonhomologous End-Joining (NHEJ)

Acc. Key	*Description*	*Gene*
Q13315	Serine-protein kinase ATM	ATM
P62805	histone H4	HIST1H4A
Q16695	histone H3.1t	HIST3H3
Q5UIP0	Telomere-associated protein RIF1	RIF1

Table 5 Nonhomologous End-Joining pathway (R-HSA-5693571)

ATM Signaling Network in Development and Disease

Acc. Key	*Description*	*Gene*
Q13315	Serine-protein kinase ATM	ATM
Q5UIP0	Telomere-associated protein RIF1	RIF1
Q13263	Transcription intermediary factor 1-beta	TRIM28

Table 6 ATM Signaling Network pathway (WP3878)

NF-kappa B signaling pathway

Acc. Key	*Description*	*Gene*
Q13315	Serine-protein kinase ATM	ATM
O43318	mitogen-activated protein kinase kinase kinase 7	MAP3K7
Q15750-1	TGF-beta-activated kinase 1 and MAP3K7-binding protein 1	TAB1

Table 7 NF-kappa B signaling KEGG pathway (hsa04064)

PROTEIN ANNOTATIONS

The protein annotations used in the xiNET crosslink viewer displays of the MRN protein complex are in Table 8, below (81, 93).

ProteinId	*AnnotName*	*StartRes*	*EndRes*	*Color*
Mre11	Nuclease and capping domain	1	411	#b0e0e6
Mre11	Rad50 interacting domain	442	477	#0000ff
Mre11	FLAG tag	712	719	#9400d3
Rad50	P-loop NTP hydrolases	3	182	#3cb371
Rad50	Mre11 interacting region	183	197	#b22222
Rad50	P-loop NTP hydrolases	198	216	#3cb371
Rad50	DelCC linker	217	223	#ffb6c1
Rad50	Mre11 interacting region	261	275	#b22222
Rad50	D-loop	357	362	#ff0000
Rad50	H-loop	386	391	#ffa500
Rad50	HA tag	433	441	#00ff00
Rad50	His6 tag	442	447	#1e90ff
Nbs1	FHA domain	2	109	#4682b4
Nbs1	BRCT I domain	114	183	#90ee90
Nbs1	BRCT II domain	216	325	#f0e68c
Nbs1	SPxK motif	432	435	#ffff00
Nbs1	Mre11 interacting region	640	662	#b22222
Nbs1	Mre11 interacting region	681	691	#b22222
Nbs1	ATM interacting region	734	754	#ff00ff

Table 8 MRN protein complex annotations

MRN COMPLEX PROTEIN SEQUENCES

The specific MRN complex protein sequences are as follows:

Mre11 protein sequence

>Mre11 (P49959) MRE11_HUMAN Double-strand break repair protein MRE11 OS=Homo sapiens GN=MRE11 PE=1 SV=3

MSTADALDDENTFKILVATDIHLGFMEKDAVRGNDTFVTLDEILRLAQENEVDFI

LLGGDLFHENKPSRKTLHTCLELLRKYCMGDRPVQFEILSDQSVNFGFSKFPWV

NYQDGNLNISIPVFSIHGNHDDPTGADALCALDILSCAGFVNHFGRSMSVEKIDIS
PVLLQKGSTKIALYGLGSIPDERLYRMFVNKKVTMLRPKEDENSWFNLFVIHQN
RSKHGSTNFIPEQFLDDFIDLVIWGHEHECKIAPTKNEQQLFYISQPGSSVVTSLSP
GEAVKKHVGLLRIKGRKMNMHKIPLHTVRQFFMEDIVLANHPDIFNPDNPKVTQ
AIQSFCLEKIEEMLENAERERLGNSHQPEKPLVRLRVDYSGGFEPFSVLRFSQKFV
DRVANPKDIIHFFRHREQKEKTGEEINFGKLITKPSEGTTLRVEDLVKQYFQTAEK
NVQLSLLTERGMGEAVQEFVDKEEKDAIEELVKYQLEKTQRFLKERHIDALEDKI
DEEVRRFRETRQKNTNEEDDEVREAMTRARALRSQSEESASAFSADDLMSIDLA
EQMANDSDDSISAATNKGRGRGRGRRGGRGQNSASRGGSQRGRADTGLETSTR
SRNSKTAVSASRNMSIIDAFKSTRQQPSRNVTTKNYSEVIEVDESDVEEDIFPTTS
KTDQRWSSTSSSKIMSQSQVSKGVDFESSEDDDDDPFMNTSSLRRNRRLGADYK
DDDDK

Nbs1 protein sequence

>Nbs1 (O60934) NBN_HUMAN Nibrin OS=Homo sapiens GN=NBN PE=1 SV=1
MWKLLPAAGPAGGEPYRLLTGVEYVVGRKNCAILIENDQSISRNHAVLTANFSV
TNLSQTDEIPVLTLKDNSKYGTFVNEEKMQNGFSRTLKSGDGITFGVFGSKFRIEY
EPLVACSSCLDVSGKTALNQAILQLGGFTVNNWTEECTHLVMVSVKVTIKTICAL
ICGRPIVKPEYFTEFLKAVESKKQPPQIESFYPPLDEPSIGSKNVDLSGRQERKQIFK
GKTFIFLNAKQHKKLSSAVVFGGGEARLITEENEEEHNFFLAPGTCVVDTGITNSQ
TLIPDCQKKWIQSIMDMLQRQGLRPIPEAEIGLAVIFMTTKNYCDPQGHPSTGLKT
TTPGPSLSQGVSVDEKLMPSAPVNTTTYVADTESEQADTWDLSERPKEIKVSKM
EQKFRMLSQDAPTVKESCKTSSNNNSMVSNTLAKMRIPNYQLSPTKLPSINKSKD
RASQQQQTNSIRNYFQPSTKKRERDEENQEMSSCKSARIETSCSLLEQTQPATPSL
WKNKEQHLSENEPVDTNSDNNLFTDTDLKSIVKNSASKSHAAEKLRSNKKREM

DDVAIEDEVLEQLFKDTKPELEIDVKVQKQEEDVNVRKRPRMDIETNDTFSDEA
VPESSKISQENEIGKKRELKEDSLWSAKEISNNDKLQDDSEMLPKKLLLTEFRSLV
IKNSTSRNPSGINDDYGQLKNFKKFKKVTYPGAGKLPHIIGGSDLIAHHARKNTE
LEEWLRQEMEVQNQHAKEESLADDLFRYNPYLKRRR

Rad50 protein sequence

>Rad50 (Q92878) RAD50_HUMAN DNA repair protein RAD50 OS=Homo sapiens GN=RAD50 PE=1 SV=1

MSRIEKMSILGVRSFGIEDKDKQIITFFSPLTILVGPNGAGKTTIIECLKYICTGDFPP
GTKGNTFVHDPKVAQETDVRAQIRLQFRDVNGELIAVQRSMVCTQKSKKTEFKT
LEGVITRTKHGEKVSLSSKCAEIDREMISSLGVSKAVLNNVIFCHQEDSNWPLSEG
KALKQKFDEIFSATRYIKALETLRQVRQTQGQKVKEYQMELKYLKQYPPAAAG
GYREMMIVMRTTELVNKDLDIYYKTLDQAIMKFHSMKMEEINKIIRDLWRSTYR
GQDIEYIEIRSDADENVSASDKRRNYNYRVVVMLKGDTALDMRGRCSAGQKVLA
SLIIRLALAETFCLNCGIIALDEPTTNLDRENIESLAHALVEIIKSRSQQRNFQLLVIT
HDEDFVELLGRSEYVEKFYRIKKNIDQCSEIVKCSVSSLGFNVHYPYDVPDYAHH
HHHH

References

1. Chessa L, Micheli R, & Molinaro A (2016) Focusing New Ataxia Telangiectasia Therapeutic Approaches. *J Rare Dis Diagn Ther* 2:2.
2. Mand MR (2015) Mechanisms and consequences of ATM activation. Dissertation (The University of Texas at Austin).
3. Shiloh Y & Ziv Y (2013) The ATM protein kinase: regulating the cellular response to genotoxic stress, and more. *Nat Rev Mol Cell Biol* 14(4):197-210.
4. Watters DJ (2003) Oxidative stress in ataxia telangiectasia. *Redox Rep* 8(1):23-29.
5. Ludwig LB*, et al.* (2013) Chromosome instability and oxidative stress markers in patients with ataxia telangiectasia and their parents. *Biomed Res Int* 2013:762048.
6. Reichenbach J*, et al.* (2002) Elevated oxidative stress in patients with ataxia telangiectasia. *Antioxid Redox Signal* 4(3):465-469.
7. Alexander A*, et al.* (2010) ATM signals to TSC2 in the cytoplasm to regulate mTORC1 in response to ROS. *Proc Natl Acad Sci U S A* 107(9):4153-4158.
8. Ditch S & Paull TT (2012) The ATM protein kinase and cellular redox signaling: beyond the DNA damage response. *Trends Biochem Sci* 37(1):15-22.
9. Guo Z, Deshpande R, & Paull TT (2010) ATM activation in the presence of oxidative stress. *Cell Cycle* 9(24):4805-4811.
10. Uttara B, Singh AV, Zamboni P, & Mahajan RT (2009) Oxidative stress and neurodegenerative diseases: a review of upstream and downstream antioxidant therapeutic options. *Curr Neuropharmacol* 7(1):65-74.
11. Lee JH*, et al.* (in press) ATM directs DNA damage responses and proteostasis via genetically separable pathways. *Sci Signal*.
12. Takahashi M*, et al.* (2013) Stress granules inhibit apoptosis by reducing reactive oxygen species production. *Mol Cell Biol* 33(4):815-829.
13. de Bruijn FJ (2016) *Stress and environmental regulation of gene expression and adaptation in bacteria* (John Wiley & Sons, Inc., Hoboken, New Jersey).
14. Guo Z, Kozlov S, Lavin MF, Person MD, & Paull TT (2010) ATM Activation by Oxidative Stress. *Science* 330(6003):517-521.
15. Shiloh Y (2003) ATM and related protein kinases: safeguarding genome integrity. *Nat Rev Cancer* 3(3):155-168.
16. Lee JH & Paull TT (2004) Direct activation of the ATM protein kinase by the Mre11/Rad50/Nbs1 complex. *Science* 304(5667):93-96.
17. Lee JH & Paull TT (2005) ATM activation by DNA double-strand breaks through the Mre11-Rad50-Nbs1 complex. *Science* 308(5721):551-554.
18. Lee JH & Paull TT (2007) Activation and regulation of ATM kinase activity in response to DNA double-strand breaks. *Oncogene* 26(56):7741-7748.
19. Sulli G, Di Micco R, & d'Adda di Fagagna F (2012) Crosstalk between chromatin state and DNA damage response in cellular senescence and cancer. *Nat Rev Cancer* 12(10):709-720.

20. Zannini L, Delia D, & Buscemi G (2014) CHK2 kinase in the DNA damage response and beyond. *J Mol Cell Biol* 6(6):442-457.
21. van Gent DC & van der Burg M (2007) Non-homologous end-joining, a sticky affair. *Oncogene* 26(56):7731-7740.
22. Kao A*, et al.* (2011) Development of a novel cross-linking strategy for fast and accurate identification of cross-linked peptides of protein complexes. *Molecular & cellular proteomics : MCP* 10(1):M110 002212.
23. Quick KL & Dugan LL (2001) Superoxide stress identifies neurons at risk in a model of Ataxia-telangiectasia. *Annals of Neurology* 49(5):627-635.
24. McKinnon PJ (2004) ATM and ataxia telangiectasia. *EMBO Rep* 5(8):772-776.
25. Semlitsch M, Shackelford RE, Zirkl S, Sattler W, & Malle E (2011) ATM protects against oxidative stress induced by oxidized low-density lipoprotein. *DNA Repair (Amst)* 10(8):848-860.
26. Stowe DF & Camara AK (2009) Mitochondrial reactive oxygen species production in excitable cells: modulators of mitochondrial and cell function. *Antioxid Redox Signal* 11(6):1373-1414.
27. Gu Z, Nakamura T, & Lipton SA (2010) Redox reactions induced by nitrosative stress mediate protein misfolding and mitochondrial dysfunction in neurodegenerative diseases. *Mol Neurobiol* 41(2-3):55-72.
28. Pallardo FV*, et al.* (2010) Mitochondrial dysfunction in some oxidative stress-related genetic diseases: Ataxia-Telangiectasia, Down Syndrome, Fanconi Anaemia and Werner Syndrome. *Biogerontology* 11(4):401-419.
29. Friedman J (2011) Why is the nervous system vulnerable to oxidative stress? *Oxidative stress and free radical damage in neurology*, (Springer), pp 19-27.
30. Reiman A*, et al.* (2011) Lymphoid tumours and breast cancer in ataxia telangiectasia; substantial protective effect of residual ATM kinase activity against childhood tumours. *Br J Cancer* 105(4):586-591.
31. Lavin MF*, et al.* (2016) Therapeutic targets and investigated treatments for Ataxia-Telangiectasia. *Expert Opin Orphan D* 4(12):1263-1276.
32. Itoh K*, et al.* (1997) An Nrf2 small Maf heterodimer mediates the induction of phase II detoxifying enzyme genes through antioxidant response elements. *Biochem Bioph Res Co* 236(2):313-322.
33. Malhotra D*, et al.* (2010) Global mapping of binding sites for Nrf2 identifies novel targets in cell survival response through ChIP-Seq profiling and network analysis. *Nucleic Acids Res* 38(17):5718-5734.
34. Darvekar SR, Elvenes J, Brenne HB, Johansen T, & Sjottem E (2014) SPBP is a sulforaphane induced transcriptional coactivator of NRF2 regulating expression of the autophagy receptor p62/SQSTM1. *PLoS One* 9(1):e85262.
35. Crighton D*, et al.* (2006) DRAM, a p53-induced modulator of autophagy, is critical for apoptosis. *Cell* 126(1):121-134.
36. Davies MJ (2016) Protein oxidation and peroxidation. *Biochemical Journal* 473(7):805-825.

37. Voos W (2013) Chaperone-protease networks in mitochondrial protein homeostasis. *Biochim Biophys Acta* 1833(2):388-399.
38. Lee J, Giordano S, & Zhang J (2012) Autophagy, mitochondria and oxidative stress: cross-talk and redox signalling. *Biochem J* 441(2):523-540.
39. Cuervo AM & Wong E (2014) Chaperone-mediated autophagy: roles in disease and aging. *Cell Res* 24(1):92-104.
40. Ciechanover A & Kwon YT (2015) Degradation of misfolded proteins in neurodegenerative diseases: therapeutic targets and strategies. *Exp Mol Med* 47:e147.
41. Rosser MF, Washburn E, Muchowski PJ, Patterson C, & Cyr DM (2007) Chaperone functions of the E3 ubiquitin ligase CHIP. *J Biol Chem* 282(31):22267-22277.
42. Lamark T & Johansen T (2012) Aggrephagy: selective disposal of protein aggregates by macroautophagy. *Int J Cell Biol* 2012:736905.
43. Yang Y & Herrup K (2005) Loss of neuronal cell cycle control in ataxia-telangiectasia: a unified disease mechanism. *J Neurosci* 25(10):2522-2529.
44. Yang Y, Varvel NH, Lamb BT, & Herrup K (2006) Ectopic cell cycle events link human Alzheimer's disease and amyloid precursor protein transgenic mouse models. *J Neurosci* 26(3):775-784.
45. Giuliano P*, et al.* (2003) DNA damage induced by polyglutamine-expanded proteins. *Hum Mol Genet* 12(18):2301-2309.
46. Boder E & Sedgwick RP (1970) Ataxia-telangiectasia. (Clinical and immunological aspects). *Psychiatr Neurol Med Psychol Beih* 13-14:8-16.
47. Savitsky K*, et al.* (1995) A single ataxia telangiectasia gene with a product similar to PI-3 kinase. *Science* 268(5218):1749-1753.
48. Butch AW, Chun HH, Nahas SA, & Gatti RA (2004) Immunoassay to measure ataxia-telangiectasia mutated protein in cellular lysates. *Clin Chem* 50(12):2302-2308.
49. Chin LS, Olzmann JA, & Li L (2010) Parkin-mediated ubiquitin signalling in aggresome formation and autophagy. *Biochem Soc Trans* 38(Pt 1):144-149.
50. Liu BQ*, et al.* (2013) BAG3-dependent noncanonical autophagy induced by proteasome inhibition in HepG2 cells. *Autophagy* 9(6):905-916.
51. Seidel K*, et al.* (2012) The HSPB8-BAG3 chaperone complex is upregulated in astrocytes in the human brain affected by protein aggregation diseases. *Neuropathol Appl Neurobiol* 38(1):39-53.
52. Carra S, Brunsting JF, Lambert H, Landry J, & Kampinga HH (2008) HspB8 Participates in Protein Quality Control by a Non-chaperone-like Mechanism That Requires eIF2 Phosphorylation. *J Biol Chem* 2009(284):5523-5532.
53. Tan JM*, et al.* (2008) Lysine 63-linked ubiquitination promotes the formation and autophagic clearance of protein inclusions associated with neurodegenerative diseases. *Hum Mol Genet* 17(3):431-439.
54. Chen W*, et al.* (2009) Differential expression of small heat shock protein 27 (Hsp27) in Ataxia telangiectasia brains. *Neurochem Res* 34(9):1658-1667.

55. Muchowski PJ & Wacker JL (2005) Modulation of neurodegeneration by molecular chaperones. *Nat Rev Neurosci* 6(1):11-22.
56. Wisniewski T & Goldman JE (1998) αB-Crystallin is Associated with Intermediate Filaments in Astrocytoma Cells. *Neurochemical Research* 23(3):385-392.
57. Gamerdinger M, Kaya AM, Wolfrum U, Clement AM, & Behl C (2011) BAG3 mediates chaperone-based aggresome-targeting and selective autophagy of misfolded proteins. *EMBO Rep* 12(2):149-156.
58. Cosentino C, Grieco D, & Costanzo V (2011) ATM activates the pentose phosphate pathway promoting anti-oxidant defence and DNA repair. *EMBO J* 30(3):546-555.
59. Matsuoka S, *et al.* (2007) ATM and ATR substrate analysis reveals extensive protein networks responsive to DNA damage. *Science* 316(5828):1160-1166.
60. Montenarh M (2016) Protein kinase CK2 in DNA damage and repair. *Transl Cancer Res* 5(1):49-63.
61. Duan Y, *et al.* (2014) HspA1A facilitates DNA repair in human bronchial epithelial cells exposed to Benzo[a]pyrene and interacts with casein kinase 2. *Cell Stress Chaperones* 19(2):271-279.
62. Quanz M, *et al.* (2012) Heat shock protein 90alpha (Hsp90alpha) is phosphorylated in response to DNA damage and accumulates in repair foci. *J Biol Chem* 287(12):8803-8815.
63. Yamamoto K, *et al.* (2012) Kinase-dead ATM protein causes genomic instability and early embryonic lethality in mice. *J Cell Biol* 198(3):305-313.
64. Olive KP, *et al.* (2004) Mutant p53 gain of function in two mouse models of Li-Fraumeni syndrome. *Cell* 119(6):847-860.
65. Bell DW, *et al.* (1999) Heterozygous germ line hCHK2 mutations in Li-Fraumeni syndrome. *Science* 286(5449):2528-2531.
66. Lee SB, *et al.* (2001) Destabilization of CHK2 by a missense mutation associated with Li-Fraumeni Syndrome. *Cancer Res* 61(22):8062-8067.
67. Daniel JA, *et al.* (2012) Loss of ATM kinase activity leads to embryonic lethality in mice. *J Cell Biol* 198(3):295-304.
68. Jacks T, *et al.* (1994) Tumor spectrum analysis in p53-mutant mice. *Curr Biol* 4(1):1-7.
69. Kadyk LC & Hartwell LH (1992) Sister Chromatids Are Preferred over Homologs as Substrates for Recombinational Repair in Saccharomyces-Cerevisiae. *Genetics* 132(2):387-402.
70. Usui T, *et al.* (1998) Complex formation and functional versatility of Mre11 of budding yeast in recombination. *Cell* 95(5):705-716.
71. Chamankhah M & Xiao W (1999) Formation of the yeast Mre11-Rad50-Xrs2 complex is correlated with DNA repair and telomere maintenance. *Nucleic Acids Research* 27(10):2072-2079.
72. Paull TT & Gellert M (2000) A mechanistic basis for Mre11-directed DNA joining at microhomologies. *P Natl Acad Sci USA* 97(12):6409-6414.

73. Borde V (2007) The multiple roles of the Mre11 complex for meiotic recombination. *Chromosome Res* 15(5):551-563.
74. Li X & Heyer WD (2008) Homologous recombination in DNA repair and DNA damage tolerance. *Cell Res* 18(1):99-113.
75. Mao Z, Bozzella M, Seluanov A, & Gorbunova V (2008) DNA repair by nonhomologous end joining and homologous recombination during cell cycle in human cells. *Cell Cycle* 7(18):2902-2906.
76. Oh J, Al-Zain A, Cannavo E, Cejka P, & Symington LS (2016) Xrs2 Dependent and Independent Functions of the Mre11-Rad50 Complex. *Mol Cell* 64(2):405-415.
77. Tauchi H, Matsuura S, Kobayashi J, Sakamoto S, & Komatsu K (2002) Nijmegen breakage syndrome gene, NBS1, and molecular links to factors for genome stability. *Oncogene* 21(58):8967-8980.
78. Brugmans L*, et al.* (2009) NBS1 cooperates with homologous recombination to counteract chromosome breakage during replication. *DNA Repair (Amst)* 8(12):1363-1370.
79. Stewart GS*, et al.* (1999) The DNA double-strand break repair gene hMRE11 is mutated in individuals with an ataxia-telangiectasia-like disorder. *Cell* 99(6):577-587.
80. Waltes R*, et al.* (2009) Human RAD50 deficiency in a Nijmegen breakage syndrome-like disorder. *Am J Hum Genet* 84(5):605-616.
81. Schiller CB*, et al.* (2012) Structure of Mre11-Nbs1 complex yields insights into ataxia-telangiectasia-like disease mutations and DNA damage signaling. *Nature structural & molecular biology* 19(7):693-700.
82. Tsubouchi H & Ogawa H (1998) A novel mre11 mutation impairs processing of double-strand breaks of DNA during both mitosis and meiosis. *Molecular and Cellular Biology* 18(1):260-268.
83. Johzuka K & Ogawa H (1995) Interaction of Mre11 and Rad50: two proteins required for DNA repair and meiosis-specific double-strand break formation in Saccharomyces cerevisiae. *Genetics* 139(4):1521-1532.
84. Falck J, Coates J, & Jackson SP (2005) Conserved modes of recruitment of ATM, ATR and DNA-PKcs to sites of DNA damage. *Nature* 434(7033):605-611.
85. Deshpande RA, Lee JH, & Paull TT (2017) Rad50 ATPase activity is regulated by DNA ends and requires coordination of both active sites. *Nucleic Acids Res* 45(9):5255-5268.
86. Williams RS*, et al.* (2009) Nbs1 flexibly tethers Ctp1 and Mre11-Rad50 to coordinate DNA double-strand break processing and repair. *Cell* 139(1):87-99.
87. You Z, Chahwan C, Bailis J, Hunter T, & Russell P (2005) ATM activation and its recruitment to damaged DNA require binding to the C terminus of Nbs1. *Mol Cell Biol* 25(13):5363-5379.
88. Park YB, Chae J, Kim YC, & Cho Y (2011) Crystal structure of human Mre11: understanding tumorigenic mutations. *Structure* 19(11):1591-1602.

89. Lee JH (2005) Characterization of the mechanisms of ATM activation by the MRN complex and DNA. Dissertation (ProQuest Dissertations Publishing).
90. Liu F, Rijkers DT, Post H, & Heck AJ (2015) Proteome-wide profiling of protein assemblies by cross-linking mass spectrometry. *Nat Methods* 12(12):1179-1184.
91. Liu F, Lossl P, Scheltema R, Viner R, & Heck AJR (2017) Optimized fragmentation schemes and data analysis strategies for proteome-wide cross-link identification. *Nat Commun* 8:15473.
92. Canman CE*, et al.* (1998) Activation of the ATM kinase by ionizing radiation and phosphorylation of p53. *Science* 281(5383):1677-1679.
93. Lee JH*, et al.* (2013) Ataxia telangiectasia-mutated (ATM) kinase activity is regulated by ATP-driven conformational changes in the Mre11/Rad50/Nbs1 (MRN) complex. *J Biol Chem* 288(18):12840-12851.
94. Paull TT & Gellert M (1998) The 3′ to 5′ exonuclease activity of Mre11 facilitates repair of DNA double-strand breaks. *Molecular cell* 1(7):969-979.
95. Paull TT & Gellert M (1999) Nbs1 potentiates ATP-driven DNA unwinding and endonuclease cleavage by the Mre11/Rad50 complex. *Genes Dev* 13(10):1276-1288.
96. Verhagen A (2006) Using FLAG Epitope-Tagged Proteins for Coimmunoprecipitation of Interacting Proteins. *Cold Spring Harbor Protocols* 2006(5):pdb. prot4557.
97. Wisniewski JR, Zougman A, Nagaraj N, & Mann M (2009) Universal sample preparation method for proteome analysis. *Nat Methods* 6(5):359-362.
98. Franz T & Li X (2015) Step-by-step preparation of proteins for mass spectrometric analysis. *Methods in molecular biology (Clifton, N.J.)* 1295:235-247.
99. Combe CW, Fischer L, & Rappsilber J (2015) xiNET: cross-link network maps with residue resolution. *Molecular & cellular proteomics : MCP* 14(4):1137-1147.
100. Consortium U (2013) Update on activities at the Universal Protein Resource (UniProt) in 2013. Nucleic Acids Res41: D43–D47.
101. Gough J, Karplus K, Hughey R, & Chothia C (2001) Assignment of homology to genome sequences using a library of hidden Markov models that represent all proteins of known structure. *Journal of molecular biology* 313(4):903-919.
102. Dowell RD, Jokerst RM, Day A, Eddy SR, & Stein L (2001) The distributed annotation system. *BMC Bioinformatics* 2(1):7.
103. Johnson M*, et al.* (2008) NCBI BLAST: a better web interface. *Nucleic Acids Res* 36(Web Server issue):W5-9.
104. Berman HM (2000) The Protein Data Bank. *Nucleic Acids Research* 28(1):235-242.
105. Notredame C, Higgins DG, & Heringa J (2000) T-Coffee: A novel method for fast and accurate multiple sequence alignment. *Journal of molecular biology* 302(1):205-217.

106. Di Tommaso P*, et al.* (2011) T-Coffee: a web server for the multiple sequence alignment of protein and RNA sequences using structural information and homology extension. *Nucleic Acids Res* 39(Web Server issue):W13-17.
107. Schrodinger, LLC (2015) The PyMOL Molecular Graphics System, Version 2.0.1.
108. Kall L, Canterbury JD, Weston J, Noble WS, & MacCoss MJ (2007) Semi-supervised learning for peptide identification from shotgun proteomics datasets. *Nat Methods* 4(11):923-925.
109. Lim HS, Kim JS, Park YB, Gwon GH, & Cho Y (2011) Crystal structure of the Mre11–Rad50–ATPγS complex: understanding the interplay between Mre11 and Rad50. *Genes & development* 25(10):1091-1104.
110. Seifert FU, Lammens K, Stoehr G, Kessler B, & Hopfner KP (2016) Structural mechanism of ATP-dependent DNA binding and DNA end bridging by eukaryotic Rad50. *EMBO J* 35(7):759-772.
111. Lammens K*, et al.* (2011) The Mre11:Rad50 structure shows an ATP-dependent molecular clamp in DNA double-strand break repair. *Cell* 145(1):54-66.
112. Consortium U (2017) UniProt: the universal protein knowledgebase. *Nucleic acids research* 45(D1):D158-D169.
113. Vaughn JL, Goodwin RH, Tompkins GJ, & McCawley P (1977) The establishment of two cell lines from the insect Spodoptera frugiperda (Lepidoptera; Noctuidae). *In Vitro* 13(4):213-217.
114. Koplin A*, et al.* (2010) A dual function for chaperones SSB-RAC and the NAC nascent polypeptide-associated complex on ribosomes. *J Cell Biol* 189(1):57-68.
115. Gregori J, Villarreal L, Sanchez A, Baselga J, & Villanueva J (2013) An effect size filter improves the reproducibility in spectral counting-based comparative proteomics. *J Proteomics* 95:55-65.
116. Yekutieli D & Benjamini Y (1999) Resampling-based false discovery rate controlling multiple test procedures for correlated test statistics. *Journal of Statistical Planning and Inference* 82(1):171-196.
117. Jakob B*, et al.* (2011) DNA double-strand breaks in heterochromatin elicit fast repair protein recruitment, histone H2AX phosphorylation and relocation to euchromatin. *Nucleic Acids Res* 39(15):6489-6499.
118. Khanna KK*, et al.* (1998) ATM associates with and phosphorylates p53: mapping the region of interaction. *Nat Genet* 20(4):398-400.
119. Hughes R (2016) p53 and Sp1 Associated RNAs Act as Non-coding Transcriptional Regulators at Homologous Loci. Masters (University of New South Wales).
120. Funayama R, Saito M, Tanobe H, & Ishikawa F (2006) Loss of linker histone H1 in cellular senescence. *J Cell Biol* 175(6):869-880.
121. Davison EJ*, et al.* (2009) Proteomic analysis of increased Parkin expression and its interactants provides evidence for a role in modulation of mitochondrial function. *Proteomics* 9(18):4284-4297.

122. Ma L, Li Y, & Wang R (2015) Drebrin and cognitive impairment. *Clin Chim Acta* 451(Pt B):121-124.
123. Spivak M, Weston J, Bottou L, Kall L, & Noble WS (2009) Improvements to the percolator algorithm for Peptide identification from shotgun proteomics data sets. *J Proteome Res* 8(7):3737-3745.
124. Walker JM (2005) *The proteomics protocols handbook* (Springer).
125. Villén J & Gygi SP (2008) The SCX/IMAC enrichment approach for global phosphorylation analysis by mass spectrometry. *Nature protocols* 3(10):1630-1638.
126. Arlt C*, et al.* (2016) Integrated Workflow for Structural Proteomics Studies Based on Cross-Linking/Mass Spectrometry with an MS/MS Cleavable Cross-Linker. *Anal Chem* 88(16):7930-7937.
127. Muller MQ, Dreiocker F, Ihling CH, Schafer M, & Sinz A (2010) Cleavable cross-linker for protein structure analysis: reliable identification of cross-linking products by tandem MS. *Anal Chem* 82(16):6958-6968.
128. Sinz A (2017) Divide and conquer: cleavable cross-linkers to study protein conformation and protein-protein interactions. *Anal Bioanal Chem* 409(1):33-44.
129. Sinz A (2006) Chemical cross-linking and mass spectrometry to map three-dimensional protein structures and protein-protein interactions. *Mass Spectrom Rev* 25(4):663-682.
130. Kapoor M (1996) How to cross-link proteins. (University of Calgary, Calgary, Canada, 2, 1N4).